TALLINN UNIVERSITY OF TECHNOLOGY
SCHOOL OF ENGINEERING
Department's title

OPTIMIZATION OF Sb_2Se_3 THIN FILM ABSORBER GROWTH PROTOCOL AND ITS APPLICATION IN SOLAR CELLS

Sb_2Se_3 ÕHUKESEKILELISE ABSORBERI KASVUPROTOKOLLI OPTIMEERIMINE JA RAKENDAMISEKS PÄIKESEPATAREIDES

MASTER THESIS

Üliõpilane: Amirhossein Palizgar

Üliõpilaskood: 184650KAYM

Juhendaja: Dr. Nicolae Spalatu
Dr. Atanas Katerski

Tallinn 2020

AUTHOR'S DECLARATION

Hereby I declare, that I have written this thesis independently.
No academic degree has been applied for based on this material. All works, major viewpoints and data of the other authors used in this thesis have been referenced.

"26th", May 2020

Author: Amirhossein Palizgar /Digitally signed/
/signature/

Thesis is in accordance with terms and requirements

"26th", May 2020

Supervisor: Dr. Nicolae Spalatu /Digitally signed/
/signature/

Accepted for defence

"26th", May 2020

Chairman of theses defence commission: Prof. Malle Krunks /Digitally signed/
/signature/

Faculty of Chemical and Material Technology

THESIS TASK

Student: Amirhossein Palizgar, 184650KAYM

Study programme, main speciality: Material and Processes of Sustinable Energetics / Processes of Sustinable Energetics

Supervisor(s): Research Scientict, Dr. Nicolae Spalatu, +3726203369
Research Scientict, Dr. Atanas Katerski, +3726203369

Thesis topic:

(in English) OPTIMIZATION OF Sb_2Se_3 THIN FILM ABSORBER GROWTH PROTOCOL AND ITS APPLICATION IN SOLAR CELLS

(in Estonian) Sb_2Se_3 ÕHUKESEKILELISE ABSORBERI KASVUPROTOKOLLI OPTIMEERIMINE JA RAKENDAMISEKS PÄIKESEPATAREIDES

Thesis main objectives:

1. To study the effect of processing conditions on the structural and morphological properties of Sb_2Se_3 seed layers deposited onto TiO_2/FTO/glass substrate.
2. To investigate the impact of the growth history of the seed layers on the grain structure of subsequent CSS Sb_2Se_3 thin film absorber.
3. To study the influence of Sb_2Se_3 absorber grown on different seed layers on the performance of Au/Sb_2Se_3/Sb_2Se_3(SL)/TiO_2/FTO/glass solar cells.
4. To study the interrelation between Sb_2Se_3 absorber morphology, thickness and Au/Sb_2Se_3/Sb_2Se_3(SL)/TiO_2/FTO/glass solar cells performance.

Thesis tasks and time schedule:

No	Task description	Deadline
1.	Deposition of TiO_2 by ultrasonic spray pyrolysis on FTO/glass.	
2.	Deposition of Sb_2Se_3 seed layer onto TiO_2/FTO/glass via HVE and CSS at different conditions.	
3.	Deposition of Sb_2Se_3 absorber layer by CSS.	
4.	Conducting material characterization techniques to study the properties of deposited Sb_2Se_3 seed layers and Sb_2Se_3 absorber films.	
5.	Solar cell performance evaluation via device characterization techniques.	

Language: English **Deadline for submission of thesis:** "26th" May 2020.

Student: Amirhossein Palizgar /Digitally signed/ "26th", May 2020
/signature/

Supervisor: Dr. Nicolae Spalatu /Digitally signed/ "26th", May 2020
/signature/

Co-Supervisor: Dr. Atanas Katerski /Digitally signed/ "26th", May 2020
/signature/

Head of study programme: Prof. Sergei Bereznev ..... "26th", May 2020
/signature/

CONTENTS

PREFACE:

The idea of the following thesis was proposed by Dr. Nicolae Spalatu, and the work was carried out in the Laboratory of Thin Film Chemical Technologies. My biggest thanks goes to him for being always open to discussion with absolute sense of responsibility and commitment. He guided me through structuring the experiment part and helped me to solve the issues I faced with. I would also like to thank Dr. Atanas Katerski for valuable discussions and technical support. Thanks to Dr. Olga Volobujeva for support with SEM measurements. I also like to express my sincere gratitude to Dr. Bereznev, who did his best to provide the best situation for my classmates and me to study this program. I'm honored to be a student in this program, and I would like to send my biggest thanks to everyone who allowed me to be a part of it. I would also like to thank Robert Krautmann for being a great help in this work.

This study was financially supported by Estonian Research Council projects under the title IUT19-4 "Thin films and nanomaterials by wet-chemical methods for next-generation photovoltaics", PRG627 "Antimony chalcogenide thin films for next-generation semi-transparent solar cells applicable in electricity producing windows" and European Regional Development Fund project TK141 "Advanced materials and high-technology devices for sustainable energetics, sensorics and nanoelectronics".

Short summary

This work is focused on optimization of Sb_2Se_3 thin film absorber growth protocol and its application in solar cells. Herein, I fabricated Au/Sb_2Se_3/Sb_2Se_3(SL)/TiO_2/FTO/glass thin film solar cells via optimization and screening of Sb_2Se_3 seed layer and Sb_2Se_3 absorber thickness. I studied the influence of various processing conditions on the morphology and structure of Sb_2Se_3 seed layers and how the growth history of the seed affects the grain structure of subsequent CSS Sb_2Se_3 absorber layer and the solar cells efficiency. I concluded that Sb_2Se_3 seed layer deposition by closed-space sublimation technique at 280 ^oC, resulted in the fabrication of the best performing Au/Sb_2Se_3/Sb_2Se_3(SL-280)/TiO_2/FTO/glass solar cell with the achieved power conversion efficiency of 4.2%. I also concluded that 2 μm (in the range of 4 to 1 μm) is the optimal thickness for the absorber layer. Therefore, the best performing Au/Sb_2Se_3/Sb_2Se_3(SL-280)/TiO_2/FTO/glass solar cells solar cell with Sb_2Se_3 absorber thickness of 2 μm with PCE of 4.9% was fabricated.

Key words: Close-spaced sublimation, Sb_2Se_3 seed layer, Sb_2Se_3 absorber layer, Thin film solar cells, Master Thesis

LIST OF ABBREVIATIONS:

PV	Photovoltaics
c-Si	Crystalline silicon
CdTe	Cadmium telluride
CIGS	Cadmium indium gallium selenide
Sb_2Se_3	Antimony Selenide
TiO_2	Titanium dioxide
CIS	Cadmium indium diselenide
α-Si	Amorphous silicon
CSS	Close-spaced sublimation
PVD	Physical vapour deposition
GBs	Grain boundaries
PCE	Photoconversion efficiency
USP	Ultrasonic spray pyrolysis
CVD	Chemical vapour deposition
PLD	Pulsed laser deposition
ALD	Atomic layer deposition
E_g	Band gap energy
TCO	Transparent conductive oxide
FTO	Fluorine-doped tin oxide
L_d	Minority carrier diffusion length
BSE	Backscattered electrons
SE	Secondary electrons
SEM	Scanning electron microscopy
XRD	X-ray diffraction
EQE	External quantum efficiency
I_{SC}	Short circuit current
V_{OC}	Open circuit voltage
M_{pp}	Maximum Power Point
HVE	High Vacuum Evaporation
SL	Seed Layer
PCE	Power conversion efficiency
PDT	Post Deposition Treatment

INTRODUCTION:

Renewable sources offer clean energy, reduce CO_2 emissions and can make us independent of fossil fuels. Among all renewable sources, solar power is the most promising source. Solar power is free, infinite, abundant and can be used to provide heat and electricity. However, harvesting this energy is a challenge that is mainly limited by technological and environmental factors. In the past few decades, different PV technologies have been developed and more technologies are expected to become available in the future. Silicon based solar cells are the most developed technologies, and can be used for large applications, but the payback period is relatively long, and possibility of decreasing fabrication costs is too low. Thus, low-cost technologies such as thin films are introduced.

The high absorption coefficient of materials used in thin film solar cells, in addition to their proper direct bandgap, allows thin films to be built with small thicknesses and less material for generation of a specific power output. CdTe and CIGS are the leading thin film technologies with the recorded efficiencies of higher than 22% [1] but, the scarcity of Tellurium and Indium as well as the presence of the toxic element of Cadmium in their fabrication processes, have raised economic and environmental concerns that limit their large-scale application. Consequently, finding earth-abundant and non-toxic raw materials, preferably compatible with the current existing fabrication methods, is the current goal in PV. Many compounds such as $Cu_2ZnSn(Se,S)_4$ [2], Sn(Se,S) [3], and $Sb_2(Se,S)_3$ are explored as alternatives to CdTe and CIGS. Among all, Sb_2Se_3 with nontoxic and earth abundant constituents has emerged as one of the most promising absorber materials due to its attractive properties such as high absorption coefficient ($>10^5$ cm^{-1}) [4] at visible spectrum, suitable bandgap of 1.1-1.3 eV, decent carrier mobility (about 10 cm^2 V^{-1} s^{-1}) [5], and simple binary composition with fixed orthorhombic phase. Sb_2Se_3 thin film solar cells have rapidly developed in the past few years and it is expected that easily reach to higher efficiencies.

Currently, the most efficient Sb_2Se_3 thin film solar cells are fabricated by closed-space sublimation (CSS). CSS is an advantageous method for Sb_2Se_3 as its high deposition rate can yield large grains with preferred orientation and low density at grain boundaries (GBs) [6]. Previous works demonstrated that Sb_2Se_3 devices performance strongly depends on the orientation of the nanoribbons on the film, and optimization of deposition conditions can achieve the optimal orientation [7]. One of the latest approaches for controlling the Sb_2Se_3 thin film absorber growth has been recently suggested by fabrication of a Sb_2Se_3 seed layer prior to absorber layer deposition.

In this work, I focused on optimization of Sb_2Se_3 thin film absorber growth via controlling Sb_2Se_3 seed layer (SL) processing conditions. Herein, I deployed High Vacuum Evaporation (HVE) and CSS to deposit 60-70 nm Sb_2Se_3(SL) at various temperatures. Different seed layer deposition methods and conditions were used in order to study how the seed layer processing condition effects the Sb_2Se_3 absorber morphology. After this, I deployed CSS to deposit Sb_2Se_3 absorber layer onto the Sb_2Se_3(SL), and studied the effect of absorber structure on Au/Sb_2Se_3/Sb_2Se_3(SL)/TiO_2/FTO/glass thin film solar cell efficiency. Finally, the effect of Sb_2Se_3 absorber layer thickness on its structural properties was analyzed and physico-chemistry of the processes responsible for the changes in the properties of the seed layers and absorber, as well as, the interrelation with the solar cell device operation were discussed.

The work starts with giving a theoretical background of working principles of solar cells, availability of PV materials, the deployed deposition techniques, and the used solar cell characterization methods. Followed by this, the experimental section is presented, where I give an overview of the Sb_2Se_3 absorber layers and TiO_2 window layers deposition processes through CSS and Spray pyrolysis technique, respectively. After fabrication of thin films, material characterization by X-ray diffraction (XRD) and scanning electron microscopy (SEM) principles were introduced. Subsequently, solar cell characterization was carried out by conducting current-voltage (J-V) and external quantum efficiency (EQE) measurements. Finally, results and processes responsible for the achieved conclusion is discussed.

1 BACKGROUND AND LITERATURE REVIEW

1.1 Basics of solar cells

Solar cells are photovoltaic devices that convert sunlight to electrical energy through the photovoltaic effect. When a solar photon is absorbed, an electron is excited if the photon energy exceeds the band gap of the semiconductor material. The junction between n-type and p-type semiconductors has electric potential, which sweeps electrons out into the external circuit. Fig. 1. shows the charge separation of light-generated carriers.

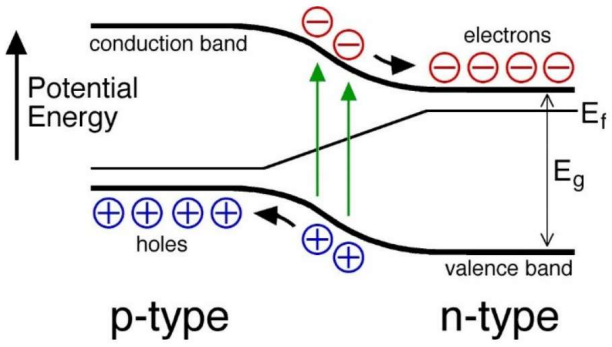

Fig. 1. Charge separation of light-generated carriers by the barrier [8]

In n-type semiconductors, the majority carriers are electrons, and in p-type semiconductors, the majority carriers are holes. When n-type and p-type materials are in contact with each other, the difference in concentrations of holes and electrons leads to diffusion. Electrons from n-type material diffuse to p-type, while holes from p-type diffuse to n-type material. As a result, a depletion region is established, where no carriers can be found, which acts as a potential barrier to further diffusion of majority carriers.

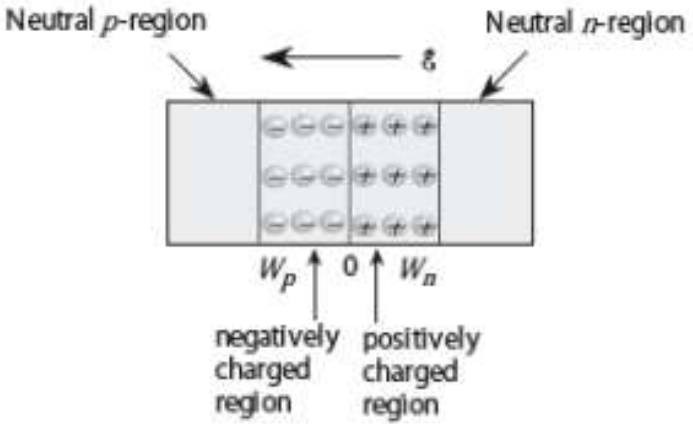

Fig. 2. Majority carriers diffusion and depletion area formation [9].

When an electron is excited, meaning it is freed from its native atom, it is subject to an electric field by the p-n junction, and the junction ensures electrons flow in only one direction.

1.1.1 Three Generation of Solar cells

Fig. 3. shows three classifications of PV cells.

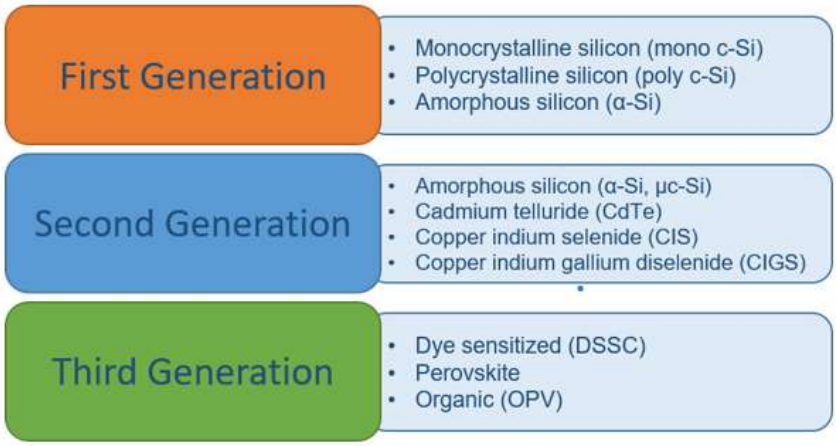

Fig. 3. Classification of Solar cells [10]

1st generation solar cells are based on silicon. Devices made by this technology can be classified into three main types depending on how the Si wafers are made [10]. Monocrystalline, polycrystalline, and amorphous silicon cells are the three types of this generation. 1st generation is the dominant and the most commercially used solar cell technology in the PV market due to their high efficiencies. Fabrication processes for this technology are relatively expensive for given output power, and solar cells made by this technology have reached the efficiencies close to their maximum theoretical value [11]. Thus, second-generation solar cells were introduced to overcome the drawbacks of the first-generation technology.

The second-generation solar cells are also known as thin film solar cells. Solar cells made by this technology have somewhat lower efficiencies compared to the 1st generation solar cells, but their fabrication processes are simpler and cheaper. 2nd generation solar cells can be fabricated on flexible substrates and large areas of up to 6 m^2 while 1st generation devices can be grown only on small dimensions [11]. Thin film solar cells are made of several thin layers that are deposited on each other. Thin film solar cells have higher absorption coefficient and can be fabricated in a vacuum and non-vacuum pressure. Meanwhile, there are concerns such as environmental contamination from fabrication processes and availability of the required materials that

do not let the technology to become the dominant one. Various materials have been used for thin films, and among all, CdTe, CIGS, CIS, and α-Si are the most widely used and developed materials [12].

The third generation of solar cells is about nano photovoltaic solar cell technologies such as nanocrystal based solar cells, polymer-based solar cells, dye-sensitized solar cells, and concentrated solar cells [11]. These are novel technologies but not yet commercially available. Each one of the third-generation solar cells looks for different approaches to reach a better efficiency/fabrication costs trade-off.

1.1.2 Thin film solar cell configuration

Thin film solar cells typically consist of two layers (absorber and window layer), which are in contact with each other and are located between the back and front contact. Window layer and front contact have similar features in terms of transparency as they are both transparent to visible light. Transparency allows sunlight to pass to the absorber layer and generate charge carriers upon absorption.

Front contact is mainly a transparent conductive oxide (TCO) film which is deposited on the surface of a substrate. Among all TCOs, indium-doped tin oxide (ITO) and fluorine-doped tin oxide (FTO) are the most commonly used materials for thin film solar cells due to being highly transparent (>80%) and having low sheet resistivity (<30 Ω/sq) [6].

Window layer is generally a n-type semiconductor, which is mostly transparent to visible light, and is mainly responsible for creating p-n junction with the absorber material. CdS, TiO_2, and ZnO are the most known materials for the window layer.

Absorber layer is responsible for generating photocarriers and separating created charges with the help of the depletion region, which exists at the interface of the window and absorber layer. The most known and widely used absorber materials for thin film solar cells are CdTe, CIGS, CIS, and α-Si [12]. Back contact is made of metal conductors that form an ohmic contact with the back of the absorber. Gold (Au), copper (Cu), or molybdenum (Mo) are the widely used materials for back contact [13]. Metal contacts extract charges into the external load.

Thin film solar cells can be fabricated in two typical configurations, as shown in Fig. 4.

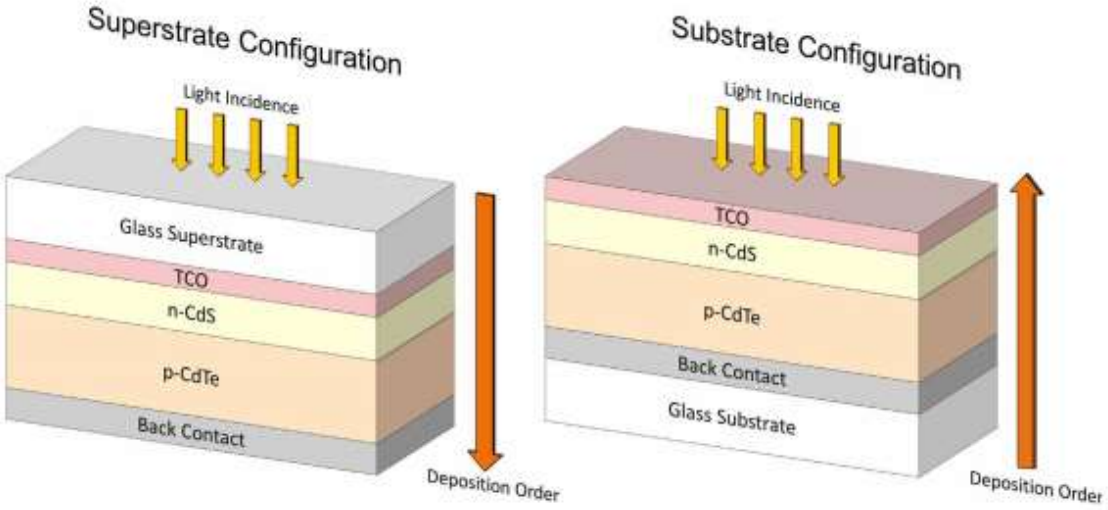

Fig. 4. Superstrate configuration (Left) and Substrate configuration (right) [14]

The main difference between these two configurations is the stacking sequence of layers. The first configuration is called superstrate, where CdS/CdTe thin film is deposited onto the TCO/glass substrate, and the second configuration is called substrate configuration, where the deposition process is in reverse order, and back contact serves as the base.

1.1.3 Photocurrent generation and collection

Photocurrent generation is dependent on three mechanisms called light absorption, charge generation, and charge recombination [15].

Light absorption

For a solar cell, light absorption happens when the energy of light photons is equal or more than the bandgap energy of the absorber material. Photons with energy less than bandgap energy do not participate in photocurrent generation as they pass through the absorber layer or get reflected.

A parameter is used to describe the probability of absorbing the energy of a photon by an absorber material. This parameter is called the absorption coefficient ($\hbar\omega$) and is an intrinsic property of a semiconductor material [16].

Photocarrier generation and charge separation

Absorption of a photon's energy by semiconductor results in the generation of an electron-hole pair. Electron is excited to the conduction band, and the hole moves to the valence band.

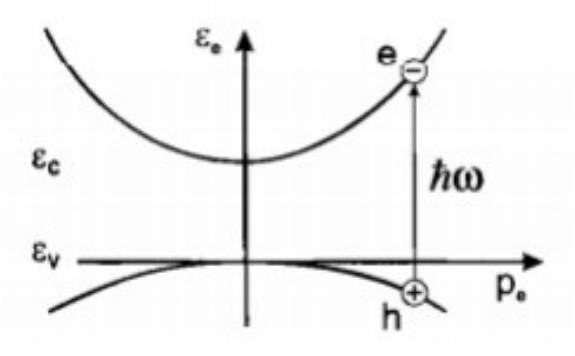

Fig. 5. Promotion of electron into the conduction band (ε_c) and hole into valence band (ε_V) by the absorption of photon with energy $\hbar\omega > E_g$ [16]

When photocarrier generation occurs in the depletion region, the electrical field moves electrons toward the n-type and holes to the p-type side. In the case of the electron-hole generation outside the depletion region, electrons and holes must reach to the depletion region to be successfully collected; otherwise, they will be recombined with majority carriers. Separation and recombination can be determined by a parameter which is called diffusion Length. Generated electrons which are more than diffusion length away of L_d from the depletion region will end up recombining while generated electrons within the diffusion length distance of L_d will be successfully separated and collected, as shown in Fig. 6. [17].

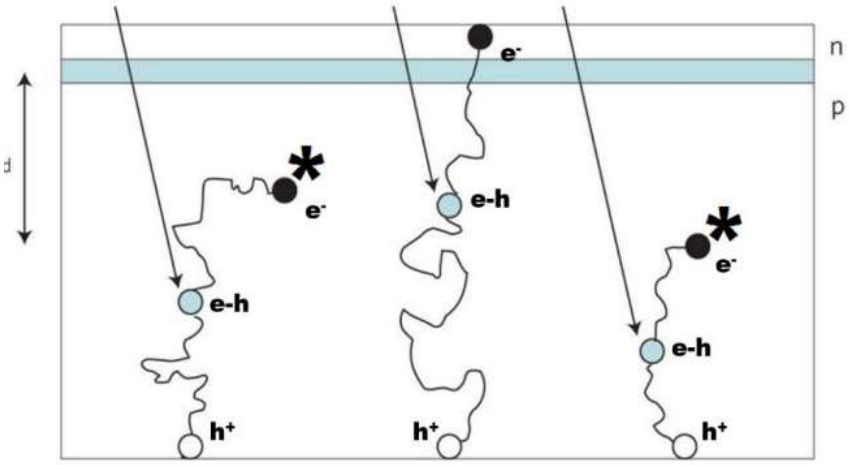

Fig. 6. Minority carrier diffusion to the depletion region. E-h pairs generated within L_d from the depletion region are collected while generated E-h pairs more than L_d from the depletion region recombine [17]

Diffusion length is an average distance that a carrier can move before recombination and is an important parameter to find the proper thickness of absorber materials. For instance, diffusion length for c-Si is L_e of ~180 μm, and this illustrates that thicknesses more than this value are redundant. In the case of Sb_2Se_3, diffusion length varies between 0.3 to 1.7 μm depending on the growth of its crystal. In general,

semiconductors that are doped significantly have shorter diffusion lengths, higher recombination rates, and shorter lifetime [18].

Photocarrier Recombination

Photocurrent recombination is an unwanted process, which annihilates the generated electron-hole pair. Therefore, it weakens the ability of a semiconductor for photocurrent generation. If an electron is not swept into the external load, it will shortly lose its energy and falls back to the valence band, where it will recombine with a hole. This process is called recombination and is classified into four main types; radiative recombination, Auger recombination, Shockley Read Hall (SRH) recombination, and surface recombination [19]. Recombination is an important issue to be addressed in order to develop high-efficiency solar cells [19].

Figure 7. shows the mechanism of radiative Recombination. In radiative recombination, an electron from the conduction band directly recombines with a hole in the valence band. It releases a photon with similar energy to the bandgap energy [20].

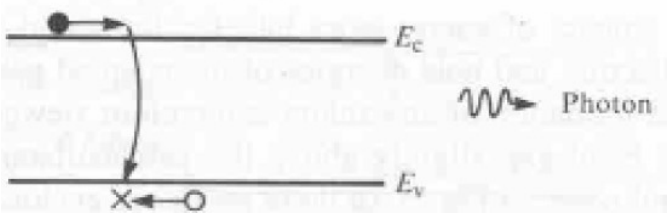

Fig. 7. Radiative recombination is known as Band-to-band recombination [20]

As shown in Figure 8, Auger recombination involves two free electrons and one hole or two free holes and one electron, respectively [21]. This type of recombination occurs when the released energy of electron-hole recombination is transferred to another carrier in the conduction band instead of being released in the form of photon or heat [22]. Auger recombination limits the lifetime and occurs mainly in heavily doped materials [23].

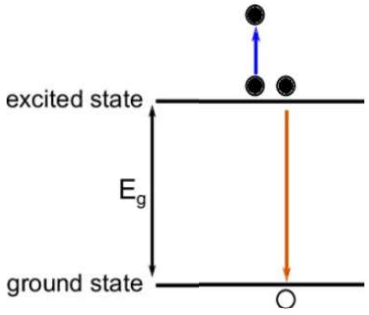

Fig. 8. Collision of two minority carriers with a same type and causing to transfer energy to another carrier [21]

Shockley Read Hall (SRH) is a recombination process that occurs due to the presence of impurities and defects in a material. SRH recombination can be reduced by choosing high-quality materials with as little number of defects as possible. Impurities such as point defects or vacancies introduce forbidden energy levels (trap levels) within the bandgap and obstruct the process of direct band-to-band generation [24]. Trap levels hold onto a single carrier, and can lead to recombination with the opposite type carrier unless the carriers thermally remitted into the conduction band [25] [23]. Figure 9. shows the mechanism of Shockley Read Hall recombination.

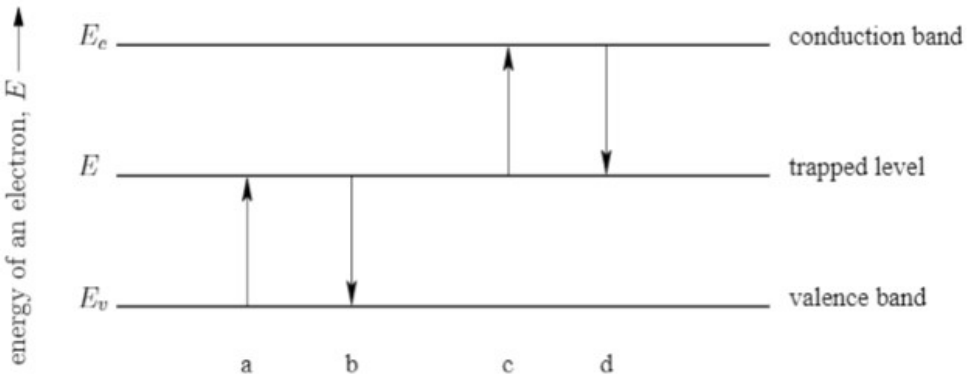

Fig. 9. The four basic processes of electron-hole recombination. a) hole emission (b) hole capture, (c) electron emission, d) electron capture [24].

SRH is more likely to happen close to the center of the bandgap energy level. If the created energy level is closer to the edge of either band, release from trap is a more likely event than recombination.

The last type of recombination is surface recombination. Surface recombination is a type of SRH recombination where the recombination occurs at the surface of solar cells due to disruptions in the crystal lattice structure. Disruptions at the surface of a lattice are inevitable, but the disruptions can be minimized through surface passivation. Passivation reduces dangling bonds that would otherwise act as potent trap states.

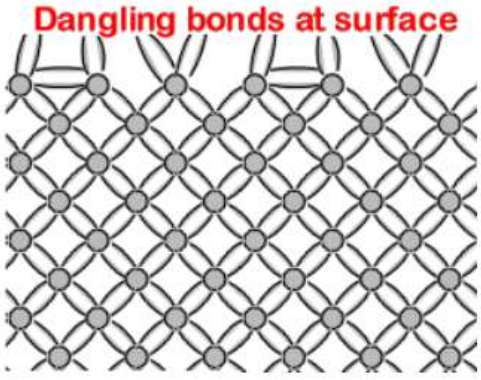

Fig. 10. Dangling bonds at the surface

1.2 Antimony selenide emerging PV technology

1.2.1 Sb_2Se_3 as an absorber material

Antimony selenide (Sb_2Se_3) is a photovoltaic absorber material that has emerged as a promising alternative to the well-known CdTe. Sb_2Se_3 is a semiconductor with a single-phase structure. It possesses attractive properties such as high absorption coefficient ($>10^5$ cm^{-1}) [4]at visible spectrum, suitable bandgap, decent carrier mobility (about 10 cm^2 V^{-1} s^{-1}) [5], long carrier lifetime and simple binary composition with fixed orthorhombic phase. These attributes, in addition to non-toxicity and earth abundancy of its constituents, are advantages that illustrate the potential to become an alternative to current thin film absorbers materials [26]. From the fabrication perspective, low temperature and vacuum-based deposition methods that have already applied for fabrication of CdTe are also applicable to Sb_2Se_3 as it possesses a low melting point of 608 °C and large vapor pressure [27] [28].

Sb_2Se_3 crystals are made of basic units of ribbon-like $(Sb_4Se_6)_n$ crystal arrays, in which the atoms are bonded through strong covalent bonds in the [001] crystal direction. However, in the [100] and [010] crystal directions Sb_2Se_3 arrays bond through weak van der Waals forces [4] [28]. The existing Van der Waals forces do not allow dangling bands to form at GBs. Thus recombination losses, which is a limiting attribute for polycrystalline PV materials, is reduced [29].

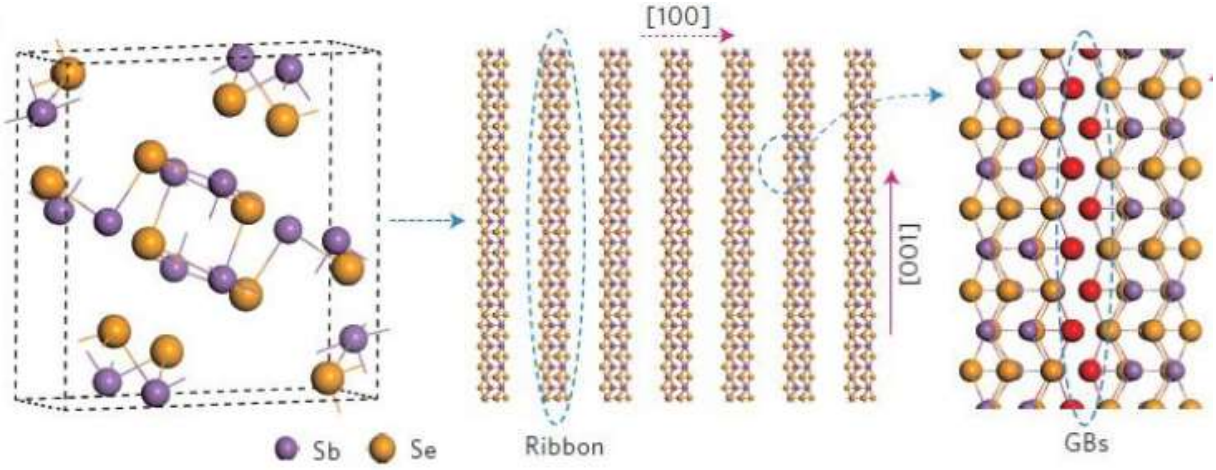

Fig. 11. Sb_2Se_3 grains growth in [001]-direction which lead to the formation of vertically stacked ribbons and reduction of dangling bonds at GBs [28]

1.2.2 Sb_2Se_3 Development

The first device that successfully deployed antimony selenide as an absorber layer for photovoltaic applications was built in 2009 by Messina and Nair et al., who utilized a solution deposition technique, and recorded the power conversion efficiency of 0.66% [30]. In early 2014, 2% efficient solar cells were fabricated, and solar cells with 3.21% power conversion efficiency were introduced later in the same year, where Sb_2Se_3 was deposited by spin coating method on TiO_2 [31]. This significant improvement in efficiency, attracted wide attention and surged interest in studying Sb_2Se_3 as a potential photovoltaic material. Further developments were made, and devices with ITO/CdS/Sb_2Se_3 structure, which were fabricated by vapor transport deposition methods, reached power conversion efficiencies of 6.5%, 7.6%, and 9.2%. In 2016, the 6.5% PCE was achieved with PbS quantum dot film as hole-transport layer [32] and the 7.6% efficiency was introduced by Wen et al. where the solar cell was fabricated by improving the crystallinity of antimony selenide by successful fabrication of the ITO/CdS/Sb_2Se_3 structure [5]. Finally, the highest efficiency was achieved in 2019, when PCE of 9.2% was recorded owing to improve in the junction interface engineering [4]. This rapid increase of the efficiency showed that Antimony Selenide surpassed the performance of binary inorganics such as FeS_2 and SnS [33], and the technology is expected to improve even further in the coming years. Although the dominant thin film technologies still overshadow Sb_2Se_3 technology, significant improvements to the absorber and the junction engineering could soon make Sb_2Se_3 based devices competitive in the PV market.

Previous works demonstrated that the device performance strongly depends on the orientation of the nanoribbons of the absorber layer and, thus far, a large part of researches made on this material has focused on optimizing growth conditions to achieve the optimal orientation [7]. It has been noted that the [211] and [221] orientations showed in better hole mobilities compared to [020] and [120], which implies the holes move across ribbons more readily than between the ribbons [28] [18] [34].

1.3 Titanium dioxide

Titanium dioxide with the chemical formula of TiO_2 is a wide band gap semiconductor. TiO_2 is used in various applications such as in solar energy conversion, water purification, photocatalysis and gas sensors [35]. TiO_2 has been widely used as electron transport layer in dye sensitized solar cells and has also been employed as window layer in thin film solar cells as a potential alternative to CdS. It is due to the fact that its

larger band gap allows more light to reach absorber. TiO_2 is chemically stable and has low toxicity.

TiO_2 can be divided into three polymorph phases with distorted TiO_6 octahedra within their crystal structure [35]. The first two phases are rutile and anatase, which have tetragonal crystal structures [36]. Brookite (Fig. 12) is the third phase with the structure corresponding to the orthorhombic system [37]. The brookite is the rarest TiO_2 in nature and the hardest phase to reach in the laboratories [38]. Thermodynamically, the rutile phase is stable at elevated temperatures, while the anatase phase is metastable [37]. However, irreversible conversion can occur from the anatase phase to the rutile phase at high temperatures. The reported band gaps for the rutile and anatase structures are 3.0 eV and 3.2 eV, respectively [37] [39].

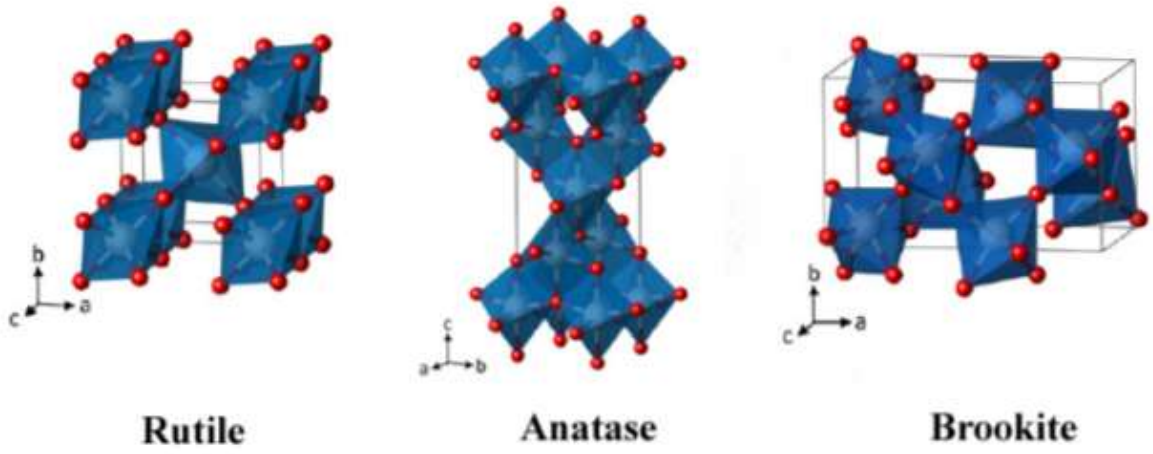

Fig. 12. Crystal Structure of TiO_2 [37]

Generally, the anatase structure is the preferred TiO_2 polymorph for solar cell applications due to potentially higher conduction band edge energy, and larger band gap [40].

1.4 Thin film deposition methods

As shown in Figure 13, thin film deposition techniques are divided into two major techniques known as physical vapour deposition and chemical vapour deposition (CVD) [41].

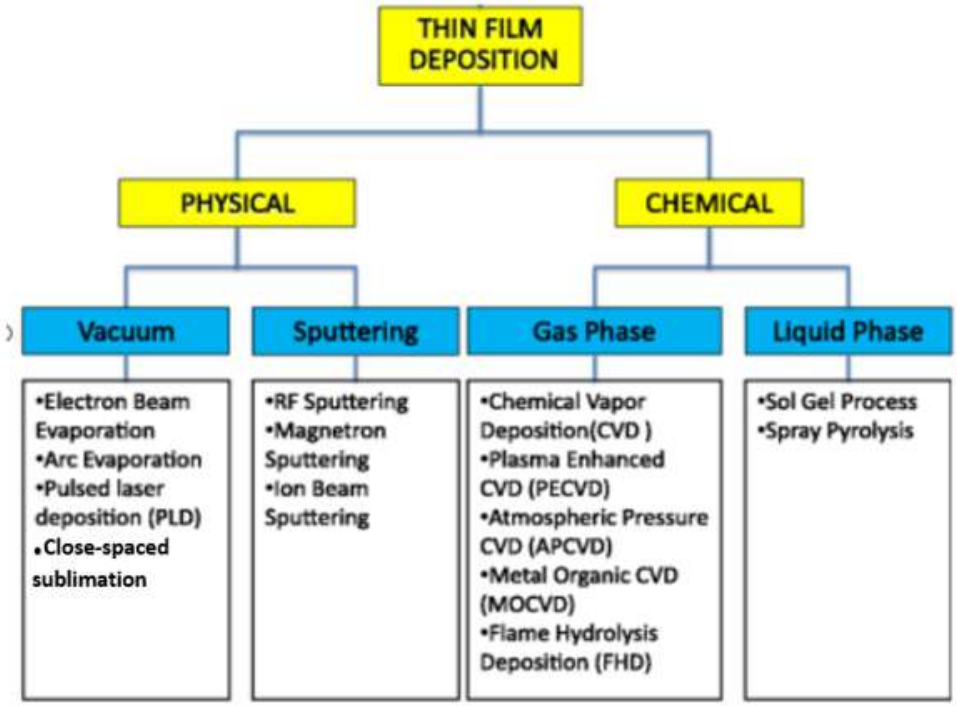

Fig. 13. Thin film deposition techniques [42]

In PVD methods, thin films are formed by condensation. Nucleation of atoms or molecules takes place on the surface of a substrate through vacuum pressure, low pressure gaseous, or plasma environment by evaporation or sputtering [41]. On the other side, CVD methods are thermodynamically processes by which the vapor undergoes a chemical reaction to fabricate a film on a substrate under specific conditions such as temperature, pressure, and reaction rate [41].

Chemical Deposition methods are classified into two different groups. In both groups, molecules of chemical compounds serving as precursors are transferred to the substrate to obtain a film. The first group deploys the gas phase, and the second group deploys a liquid for transporting molecules to the surface of the substrate. Therefore, they are known as gas phase and liquid phase techniques, respectively.

Gas-Phase deposition techniques contain two main methods: chemical vapour deposition (CVD) and atomic layer epitaxy (ALE).

Chemical Solution Deposition or Sol-Gel Processing, in addition to different methods such as Dip coating, spin coating, and Spray Pyrolysis, are techniques that belong to the Liquid phase class.

Here we deployed a PVD technique for deposition of our absorber layer while a CVD technique was used for fabrication of the TiO_2 window layer. Different deposition techniques such as Chemical Vapour Deposition [43], dip coating, Pulsed Laser Deposition (PLD) [44], Sol-gel and Ultrasonic Spray pyrolysis [45] have been used for

fabrication of TiO_2 thin films, and Spray pyrolysis is known to be one of the simplest techniques. Reports have shown that deploying Spray pyrolysis for deposition of TiO_2 films at temperatures higher than 400 °C mainly leads to the fabrication of films with the anatase phase. Deploying the Sol-gel spin-coating deposition at temperatures below 300°C leads to an amorphous structure. However, further annealing at higher temperatures will cause a structural transformation to the anatase phase. Furthermore, increasing the annealing temperature to more than 700 °C changes the structure to the rutile phase [46] [47] [48] [44]. Among all techniques, Ultrasonic Spray Pyrolysis has attracted attention because of being a simple, convenient, cost-effective, and applicable method for large area deposition.

1.4.1 Close-spaced sublimation (CSS)

Close-spaced sublimation (CSS) is the simplest physical evaporation method used for fabrication of thin films. Through this method, solid materials are deposited onto a substrate in high vacuum [49]. CSS has high deposition rate and can be simply scaled up for large scale manufacturing purposes [50]. As an example, a 1-10 μm layer of Cadmium Telluride can be coated within 10 minutes at the temperature of 600 ^{o}C [49]. Thus, it is known to be one of the fastest techniques among all Physical Vapour depositions. CSS technique can be used for the coating of semiconductor materials with an evaporation temperature of less than 800 ^{o}C [49].

One of the most important requirements for designing a close-spaced sublimation system is to minimize the influence of impurities in the deposition process so that the number of impurities would be reduced and not be heated/deposited on the films [49]. Various parameters affect the deposition process and the properties of fabricated films. Therefore, CSS equipment can be built along with various options like spacing between source and substrate, temperature, and vacuum. The schematic view of the CSS system is shown in Figure 14.

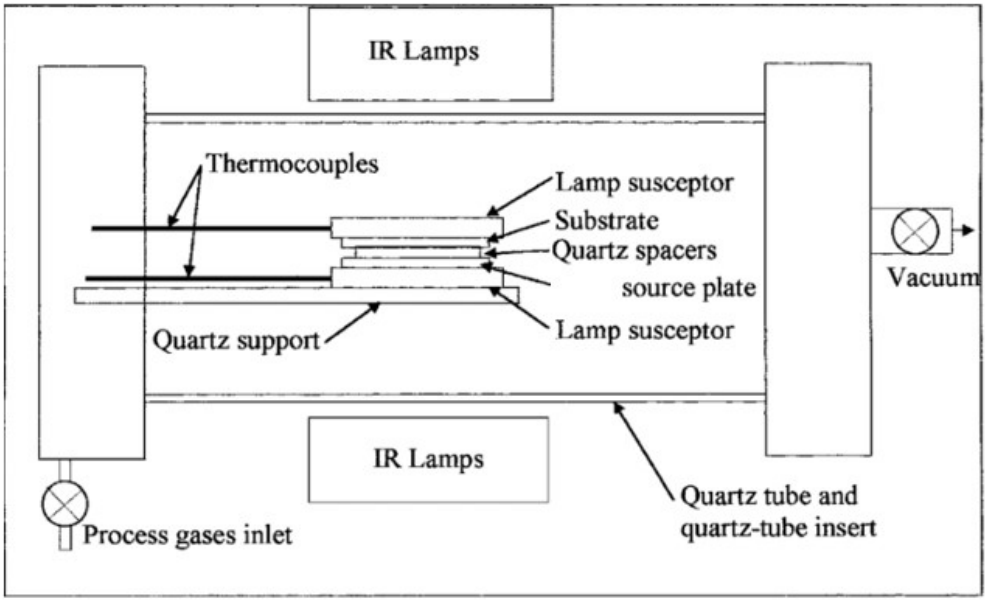

Figure 14. Close-spaced sublimation schematic view [51]

Before deposition, a rotary oil pump and diffusion pump are used to achieve a high vacuum in the reaction chamber. Rotary oil pump changes the pressure to 10^{-4} Torr and then, the diffusional pump applies higher vacuum pressure within the range of 10^{-6} Torr. The reaction chamber is the place where the substrate and the source material are kept in a specific distance from each other and also kept in the place that all the evaporation process takes place. Reaction chamber walls are covered with quartz to ensure that contaminations from graphite are not involved in the deposition processes [52].

The deposition process starts with heating up a solid material to its vaporization temperature and ends when the vaporized particles are condensed on the substrate. The substrate is also heated up during the deposition, but its temperature is kept lower than the source material to allow the condensation of vapor particles to take place. The whole process is maintained in a high vacuum to assure that only the source material is deposited and contamination is not involved in the process. Thermocouples are also implemented in the source and the substrate to monitor the temperature of the source and the substrate. The crystalline structure of fabricated thin films is dependent on various parameters such as the distance between the source and targeted material, the substrate temperature, the source temperature, evaporation temperature, the composition of the source material, and the gas pressure [5]. Commonly, in the CSS technique, deposition takes place at pressures between 1 to 30 Tor, the substrate temperature of 500 to 600 ^{o}C, and source temperature of 700 and 800 ^{o}C [49].

1.4.2 Chemical spray pyrolysis

Chemical Spray Pyrolysis is a fast, simple, non-vacuum required, and low-cost chemical deposition technique that can be used for the fabrication of metal sulphide and oxydes thin films [53] [54]. This method is a solution-based technique by which chemical compounds in a proper solvent (called precursor solution) are sprayed on a pre-heated substrate, where thermal decomposition appears, and the constituents react to form a chemical compound [55]. The main equipment to conduct the spray pyrolysis method is a precursor solution, an atomizer, a substrate heater, and temperature controllers [56].

Spray Pyrolysis starts with converting precursor solution into droplets through a nozzle and assisting them to be transported on a heated substrate. After reaching to the surface of the substrate, high temperature leads to evaporation of the solvent and thermal decomposition of the precursor. Fig. 15. shows the setup of this method.

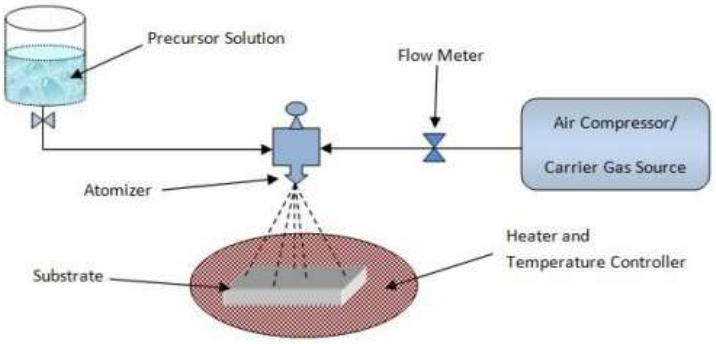

Fig 15. Spray pyrolysis schematic [16]

Various parameters influence on properties of fabricated films such as substrate temperature, spray rate, and ambient pressure. Among them, the temperature of the substrate is the most important factor [57]; because droplets drying, decomposition and grain growth is strongly dependent on this parameter [54]. Other parameters such as the concentration of precursor solution, carrier gas flow rate, nozzle-to-substrate distance, and evaporation rate must also be controlled to reach a desired crystalline structure and thickness [57].

The advantages of Spray pyrolysis compared to other methods are:

- Cost-effective.
- Simple, no special conditions
- Relatively uniform and high-quality coating.
- Reproducible of films due to its potential for mass production.
- The ability of coating complex samples
- No need for high temperature

1.5 Material characterisation methods

1.5.1 X-ray Diffraction (XRD)

X-ray diffraction is a non-destructive and standard method used for analyzing crystal structure, atomic spacing, and phase composition of materials [58]. This method was traditionally used for thick materials and materials in the form of powder since X-rays arrays have a high ability to penetrate materials. XRD makes an important role in the characterization of materials due to many materials being in various forms other than single-crystal. Figure 16 shows the schematic of XRD.

X-ray diffractometers are made of three parts: An X-ray tube, a holder to hold the sample, and a detector. In this technique, a monochromatic beam of X-ray strikes on a sample, and the interaction of the projected X-ray beams with the sample leads to the production of diffracted beams [59]. The diffracted beams with various reflection intensities will be collected by a detector to determine the sample's crystal structure. However, several orientations must be collected for reaching to a true determination over the crystal structure.

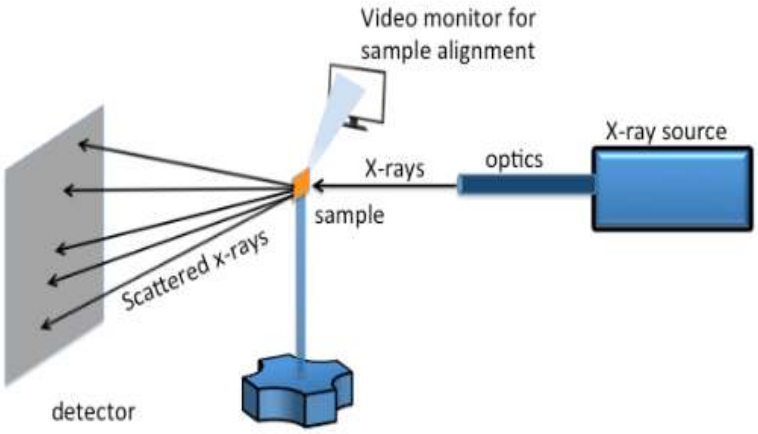

Fig. 16. Schematic illustration of XRD [59]

X-ray diffraction is based on Bragg's law (Equation 1), where d is the distance between parallel crystal planes of the sample, lambada (λ) is the incident x-ray wavelength, n is an integer called the order of reflection and theta is the angle between the beam and the plane [59]. The law states that constructive interference between 2 reflected X-rays from crystal planes occurs when the phase difference is an integer multiple of wavelengths [60].

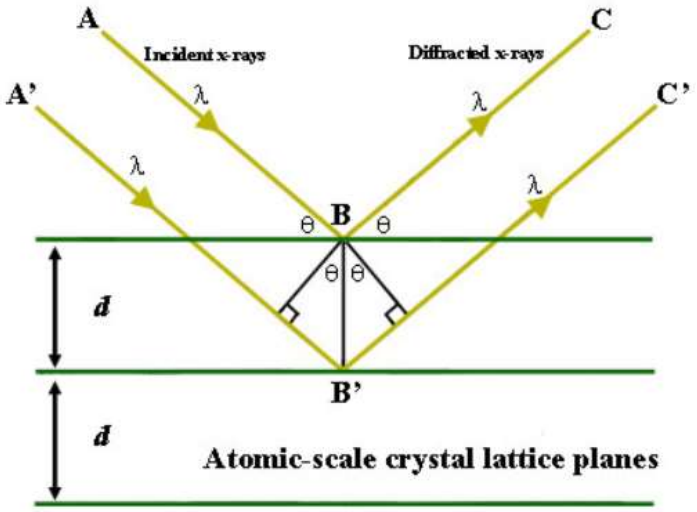

Fig. 17. Bragg's Law reflection where path difference is 2dsin Θ and d denotes the inter-planar distance [61].

The projected X-ray waves interact with atoms in crystals of the sample and interfere with the others as they leave the crystal. The interference occurs due to different reflections from each atomic plane in the crystal structure, and the diffraction occurs when Bragg's law is satisfied by constructive interference. The diffracted X-rays are collected continuously while the sample and detector are continuously rotating. The recorded intensities are commonly plotted against the angle of projected X-ray, and a series of peaks are produced. These peaks represent the angle at which the crystal planes with interplanar distance (d) diffracted X-rays that interfered constructively.

$$n\lambda = 2d \sin\theta \qquad (1)$$

These diffraction patterns are matched with previously determined diffraction patterns for respective material.

1.5.2 Scanning Electron Microscopy (SEM)

Scanning Electron Microscopy is an analysis technique that has been extensively used for studying structural and topological properties of samples [62]. The method is a non-destructive technique that uses electrons to provide high resolution, large depth field, and three-dimensional images. SEM scans various signals at the surface of a sample when a focused electron beam is projected to it. Signals are originated from interactions between the electrons in the beam and the sample. These signals reveal information on the structure of the sample and will be collected to create an image of the sample. A schematic representation of an SEM is shown in figure 18.

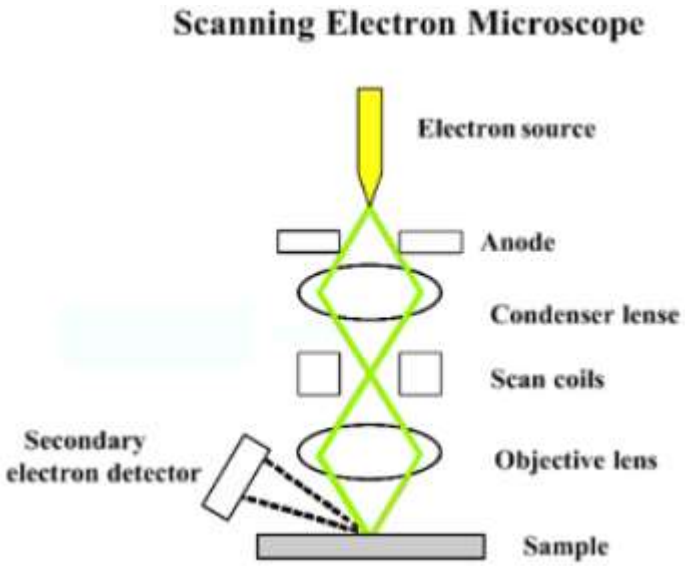

Fig. 18. schematic representation of the basic SEM components [63] [62]

Electrons of the focused beam have high kinetic energy and can produce elastic or inelastic reactions with atoms of the sample. These reactions lead to the generation of valuable emissions such as secondary electrons, backscattered electrons, heat, and visible light [64].

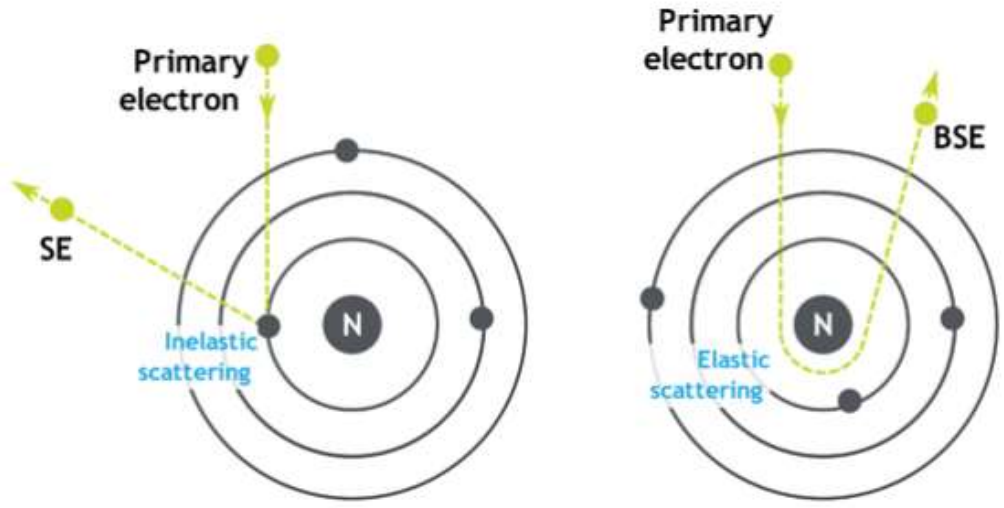

Fig. 19. Formation of Secondary Electrons (left) and Backscattered Electrons(right) [65]

Secondary electrons provide the most valuable information about the topography and surface properties of the specimen. SE is generated due to inelastic reactions between the sample and beam electrons. The projection of the primary beam leads to the dislodging of an electron from the inner shell atom of the sample. Therefore, the energy level of secondary electrons is small (2-5 eV) as a major part of their energy being released after the collision [66]. This means that secondary electrons can be collected close to the surface.

Backscattered (BSE) electrons are electrons of the primary beam that are reflected back after elastic interaction with the nucleus of the atom of the sample. These negatively charged electrons circle the nucleus and come back out of the sample instead of being captured by the positive nucleus. Backscattered electrons provide valuable information on the sample's composition and distribution of different chemical phases.

1.6 Solar cell characterization methods

1.6.1 Current-Voltage (J-V) Curve

Solar cells behave similarly to diodes as they both generate photocurrent under illumination. A solar cell produces photovoltage when the device is illuminated, and an external load is connected to it [67] . Solar cells generate DC current, and multiplying voltage to the current gives the output power. The equivalent circuit of a solar cell is shown in Figure 20. [67], where light-induced photocurrent source (I_L) is in parallel with the diode, producing opposing diffusion current (I_D) and shunt resistance producing opposing shunt current (I_{sh}). Shunt Resistance (R_{SH}) has a significant share in power losses as it provides an alternative path for photo-generated current. Series Resistance (R_S) is the other parameter that contributes in power losses. In an ideal solar cell, R_{SH} and R_S tend to infinite and zero, respectively.

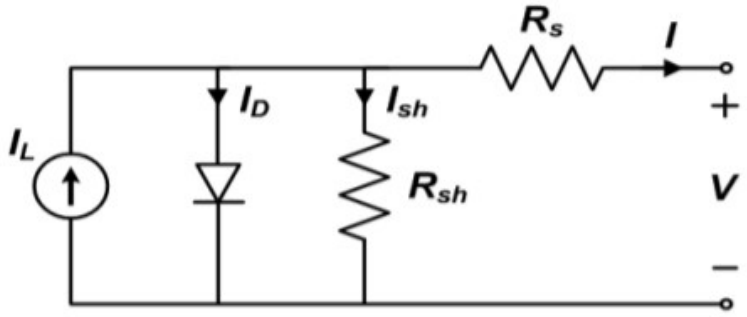

Fig. 20. Equivalent circuit of a solar cell [67]

The main electrical characteristics of solar cells are Short Circuit Current (I_{SC}), Open Circuit Voltage (V_{OC}), Fill Factor (FF), Power Conversion Efficiency (PCE). The mentioned parameters, along with the required information for the configuration of a solar system, can be extracted from an I-V curve. Fig. 21. shows a typical I-V curve for a solar module under normal conditions.

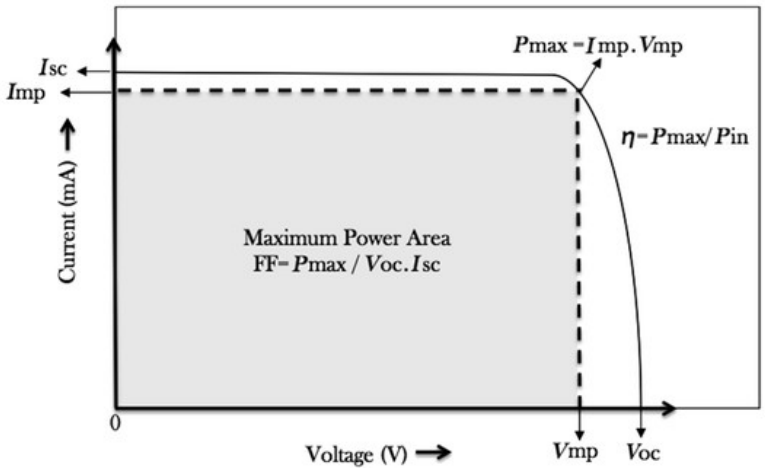

Fig. 21. A typical I-V curve of solar cells [68]

The key Parameters of I-V curves are Open Circuit Voltage (V_{OC}) and Short Circuit Current (I_{SC}) [68]. At open circuit conditions, no load is connected to the solar cell, while at the short circuit condition, the positive and negative sides of the solar cell are connected together.

Open-circuit voltage shows the threshold voltage at which the diffusion current neutralizes the generated photocurrent. Short-circuit current shows the maximum current that a solar cell can produce. In an ideal situation, an I-V curve should have a rectangular shape with the theoretical peak power being the product of V_{oc} and I_{sc}. However, in reality, I-V curves are curve-like, and generated powers are less than their theoretical peak power values. At a specific point near the bend point of the I-V curve, where $I=I_{mp}$ and $V=V_{mp}$, the maximum power is extracted from the solar cell. This point is known as the maximum power point (M_{pp}) [68].

Fill factor is a parameter that can be used to measure the quality of a solar cell. This parameter refers to the squareness of an I-V curve [25]. Fill factor is given by equation 2, where J_{mp}, V_{mp}, J_{SC} and V_{OC} are the maximum point for current density, maximum point for voltage, short circuit current density and the open-circuit voltage, respectively:

$$FF = \frac{J_{mp}\, V_{mp}}{J_{SC}\, V_{OC}} \qquad (2)$$

PCE is defined as the ratio of maximum generated power to the theoretical peak power (equation 3) [69]. PCE is dependent on various parameters, such as irradiation levels and temperature [68]. This parameter is one of the most common parameters for comparing the performance of two different solar cells.

$$PCE = \frac{J_{mp}\, V_{mp}}{P_S} \qquad (3)$$

1.6.2 External quantum efficiency

External quantum efficiency (EQE) measurement is an important technique to observe solar cell behavior in a specific range of wavelength [70]. EQE is defined to describe the ratio of collected carriers by a solar cell to the number of incident light photons on the solar cell [71]. Figure 22 presents a sample of the EQE curve.

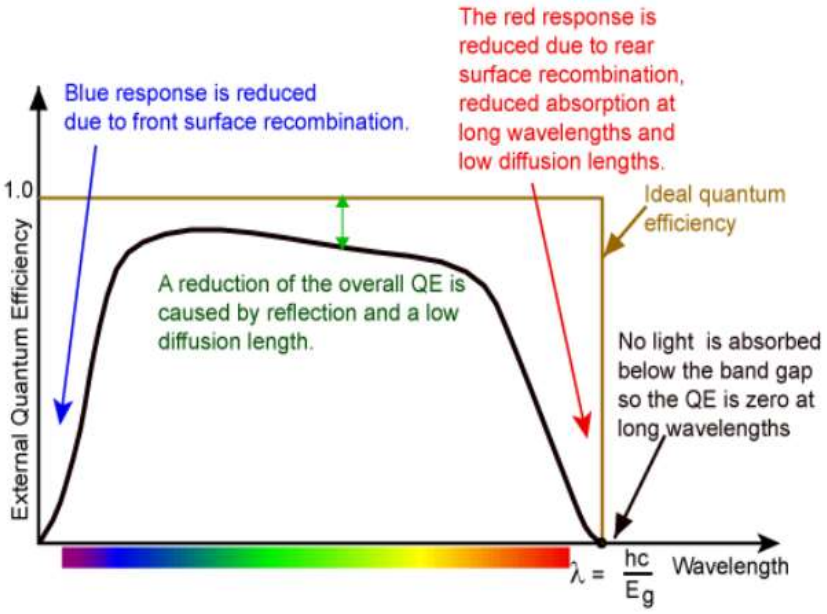

Fig. 22. A typical EQE graph [72] [73]

Ideally, EQE is in a square shape, but most solar cells do not have this shape due to recombination effects. Material properties such as absorption coefficient and charge separation/collection efficiencies, significantly influence on EQE.

1.7 Summary of theoretical background and aims of the thesis

Based on the literature review, the following key points can be presented:

1. Sb_2Se_3 is a promising photovoltaic absorber material due to its suitable bandgap of 1.1-1.3 eV and high absorption coefficient (>10^5 cm^{-1}). Sb_2Se_3 has a 1D crystal structure composed of nano ribbons allowing high carrier mobility (about 10 cm^2 V^{-1} s^{-1}).
2. Sb_2Se_3 can be deposited through vacuum-based deposition techniques which have already applied for deposition of CdTe.
3. TiO_2 is the most attractive alternative to CdS due to its chemical stability, high optical transmittance, and non-toxicity of its constituents
4. The growth of [221] and [211] oriented Sb_2Se_3 absorber films are preferred as it improves the carrier transport in solar cell devices.
5. The current strategy in development of Sb_2Se_3/TiO_2 focuses toward controlling the growth of the absorber grains to obtain the [221] and [211] preferred orientations.
6. Controlling of the Sb_2Se_3 thin film absorber growth via application of seed layer represents the recent focus in the development of Sb_2Se_3 PV technology. The investigation in this area is at the very beginning stage and systematic studies are required on this topic.

Aims of the thesis are as follow:

1- To gain knowledge of CSS and Spray Pyrolysis deposition techniques for fabrication of thin films and solar cells.
2- To get acquainted with material and device characterisation methods.
3- To study the effect of processing conditions on the structural and morphological properties of Sb_2Se_3 seed layers deposited onto TiO_2/FTO/glass substrate.
4- To investigate the impact of the growth history of the seed layers on the grain structure of subsequent CSS Sb_2Se_3 thin film absorber.
5- To study the influence of Sb_2Se_3 absorber grown on different seed layers on the performance of Au/Sb_2Se_3/Sb_2Se_3(SL)/TiO_2/FTO/glass solar cells.
6- To study the interrelation between Sb_2Se_3 absorber morphology, thickness and Au/Sb_2Se_3/Sb_2Se_3(SL)/TiO_2/FTO/glass solar cells performance.

2 EXPERIMENTAL

2.1 Fabrication of Au/Sb_2Se_3/Sb_2Se_3(SL)/TiO_2/glass solar cell

Figure 23 shows the schematic representation of our fabricated thin film solar cells with superstrate configuration.

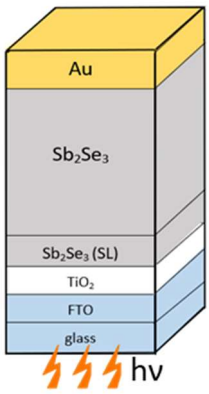

Fig. 23. Schematic of Au/Sb_2Se_3/Sb_2Se_3(SL)/TiO_2/FTO/glass superstrate configuration solar cells

Glass/FTO substrate preparation

The chosen substrates were Soda-lime glasses with coated fluorine-doped tin oxide (FTO). The FTO thickness was in the range of ~200nm and with a typical sheet resistance of ~25 Ω/sq. The substrates were prepared through two major steps; The first step was to cut the Glass/FTO to 20 x 20 mm area, and the second step was cleaning the substrates. For cleaning purposes, the 20 x 20 mm Glass/FTO substrates were sunk into a solution of 10 g $K_2Cr_2O_7$ + 10 mL H_20 + 100 mL H_2SO_4. After 2-3 hours of remaining in the solution, the substrates were washed by deionized water and moved to an ultrasonic bath of deionized water for 10 minutes, and were dried with compressed air.

Deposition of TiO_2 by Spray Pyrolysis

Fabrication of the window layer was carried out by deposition of TiO_2 onto Glass/FTO substrates, where the Spray pyrolysis technique was used. Here, I used a precursor solution of Titanium (IV) isopropoxide (TTIP) with the chemical formula of $C_{12}H_{28}O_4Ti$ and Acetylacetone (AcAc). TTIP and AcAc were dissolved in ethanol with the molar ratio of 1:4 to prepare a 50 ml spray solution. The substrate temperature was set to 340 ^oC, and compressed air with 5 L/min was used as the carrier gas. Deposition took place for 15 minutes, and the deposited TiO_2 films were subjected to post deposition treatment for 30 minutes at 450 ^oC

Sb_2Se_3 seed layer deposition

In this work, two methods were used for Sb_2Se_3 seed layer deposition. In the first method, close-spaced sublimation was used to deposit Sb_2Se_3 seed layers at various temperatures from 280 to 350 °C. In the second method, the Sb_2Se_3 seed layer was deposited by High Vacuum Evaporation (HVE), and subjected to post-deposition treatment for 30 min at 400 °C, in N_2 atmosphere.

Sb_2Se_3 absorber layer deposition

Fabrication of the absorber layer was done by Close spaced sublimation of Sb_2Se_3 onto the Sb_2Se_3(SL)/TiO_2/FTO/glass. Herein, the substrate temperature was kept at 460 °C and the source temperature was set to 490 °C in order to allow the deposition to takes place with the rate of 1 μm/min.

2.2 Material characterization

Scanning electron microscopy

A Zeiss EVO-MA15 scanning electron microscope (SEM) equipped with Zeiss HR FESEM Ultra 55 system was used for visualization of crystal growth and crystal structure.

X-ray diffraction

X-ray diffraction (XRD) was carried out to analyze the phase decomposition and crystallographic properties of Au/Sb_2Se_3(SL)/TiO_2/FTO/glass thin film solar cells. The measurements were done by using a Rigaku Ultima IV system with monochromatic Cu Kα radiation (λ = 1.5406 Å, 40 kV at 40 mA) which was equipped with a D/teX Ultra silicon line detector in the 2θ [52]. The extracted XRD patterns were studied further by Rigaku PDXL software to calculate crystal sizes and lattice constants.

2.3 Characterization of solar cells

Here, I used current-voltage characteristics (J-V) and external quantum efficiency methods (EQE) to analyze the fabricated AU/Sb_2Se_3(SL)/TiO_2/FTO/glass thin film solar cells. I extracted J-V curves by deploying an AUTOLAB PGSTAT 30 and an Oriel class A solar simulator 91159A. All the measurements were carried out under the standard illumination intensity of 100 mW/cm^2, AM1.5G.

The EQE measurements were carried out in the spectral region of 300-1100 nm by using a 300 W Xenon lamp and a computer-controlled SPM-2 monochromator (Carl Zeiss-Jena) at 30 HZ. All the device measurements were carried out at the Laboratory of Thin Film Chemical Technologies of Tallinn University of Technology.

3 RESULTS AND DISCUSSION

Section 3.1-3.2 report on the results of systematic studies on the effect of deposition conditions on the structural and morphological properties of Sb_2Se_3 seed layer deposited onto TiO_2/FTO/glass substrate and how the growth history of the seed layers influences the grain structure of subsequent CSS Sb_2Se_3 thin film absorber layers. Herein, screening experiments were conducted to identify the optimal deposition conditions of Sb_2Se_3 seed layers in order to develop Sb_2Se_3 absorber layers with optimal orientation and suitable grain structure for application in Sb_2Se_3 based thin film solar cells. The influence of deposited Sb_2Se_3 thin film absorbers via various seed layers as well as the effect of the Sb_2Se_3 absorber thickness on the efficiency of Sb_2Se_3 thin film solar cells were investigated. Physico-chemistry of the processes responsible for the changes in the properties of the seed layers and absorber, and the interrelation with the solar cell device operation are discussed.

3.1 Influence of Sb_2Se_3 seed layer processing conditions on structural and morphological properties of Sb_2Se_3 thin film absorber

To study the effect of Sb_2Se_3 seed layers (SL) deposition condition on the structural and morphological properties of the Sb_2Se_3 absorber layer, a large series of samples were deposited. Part 3.1.1 reports on the effect of samples where the corresponding Sb_2Se_3(SL) was deposited by close space sublimation, and the deposition temperature was varied from 250 to 350 °C. Afterward, Part 3.1.2. and 3.1.1 are presented, where the effects of Sb_2Se_3(SL) deposited by High Vacuum Evaporation (HVE) and the effects of Sb_2Se_3 absorber thickness deposited onto CSS Sb_2Se_3(SL)/TiO_2/FTO/glass substrates were studied, respectively.

3.1.1 Effect of Sb_2Se_3 seed layers by CSS

Figure 24. shows SEM images of Sb_2Se_3(SL) and absorber films deposited by CSS onto TiO_2/FTO/glass and Sb_2Se_3(SL)/TiO_2/FTO/glass substrates, respectively. In the top-view SEM image of the sample without the Sb_2Se_3 seed layer (Fig. 24. a) being deposited, rounded-like grain shapes can be detected. This shape is commonly observed when TiO_2 films are deposited by USP on top of FTO/glass substrates [74]. As can be seen in the cross-sectional SEM image of the same film (Fig. 24. b), fabricated Sb_2Se_3 absorber layer contains grains with small sizes and randomly oriented. Grains are tilted and are not aligned in a specific direction. Thereafter, the Sb_2Se_3 seed layer was deposited by

CSS onto TiO_2/FTO/glass in order to study how it would affect the Sb_2Se_3 absorber layer growth. Figure 24. c presents the top view of the structure where the Sb_2Se_3(SL) was deposited at 250 °C on the TiO_2/FTO/glass. Herein, the seed layer covered the surface of the TiO_2 layer and slightly improved the Sb_2Se_3 absorber grains structure. Herein, Sb_2Se_3 absorber grains are more uniform and have larger sizes.

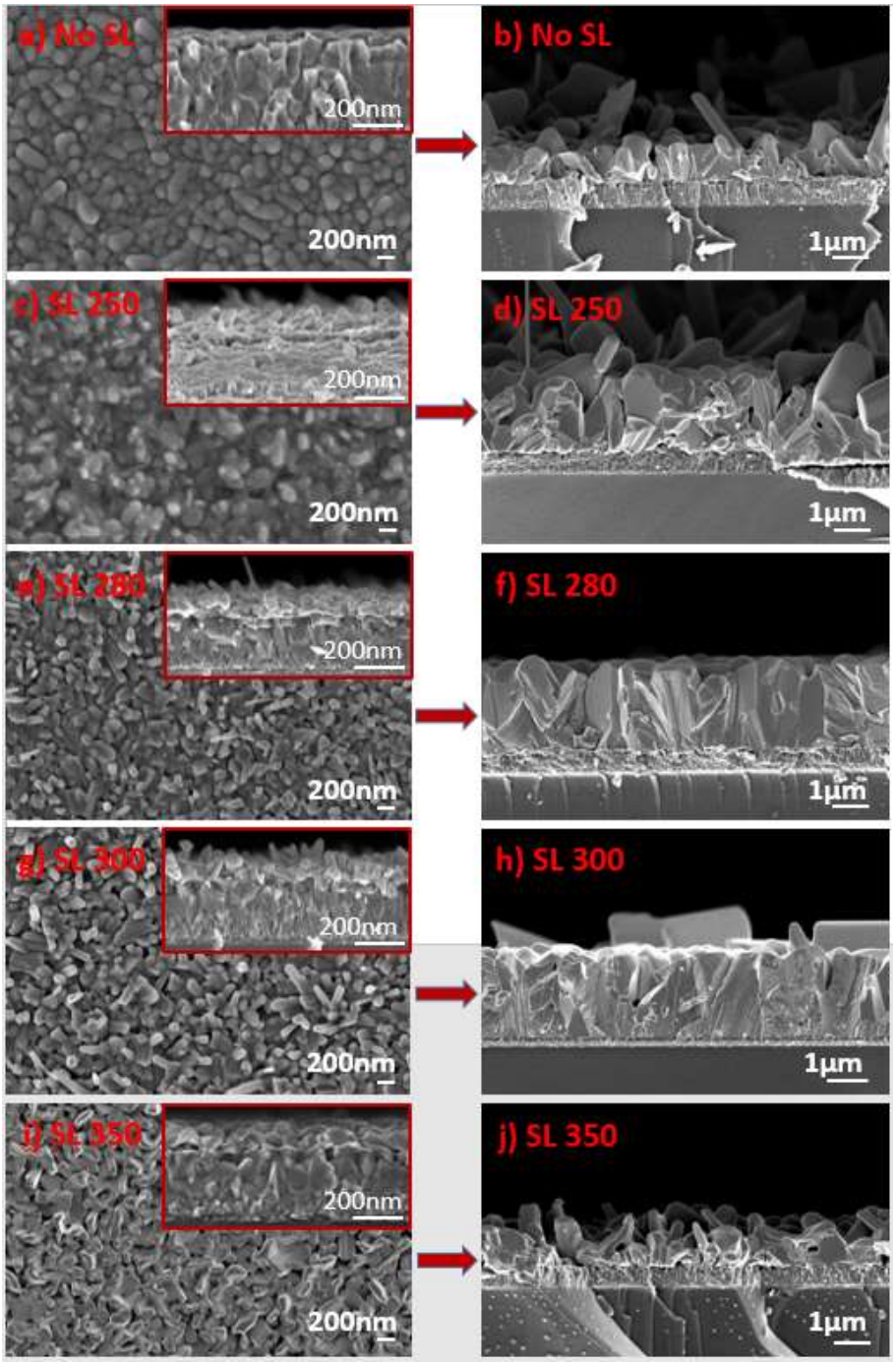

Fig. 24. SEM images of Sb_2Se_3 seed layers (SL) and absorber films deposited by CSS onto TiO_2/FTO/glass and Sb_2Se_3(SL)/TiO_2/FTO/glass substrates, respectively. Left: top view (inset, cross view) of (a) TiO_2/FTO; (c, e, g, i) Sb_2Se_3 SL deposited at temperatures between 250 and 350 °C. Right: (b, d, f, h, j) cross-sectional view of Sb_2Se_3 absorber films grown at 470 °C on corresponding Sb_2Se_3 SL (c, e, g, i).

Increasing the SL deposition temperature from 250 to 280 °C resulted in the generation of Sb_2Se_3 nanorods on the surface of the substrate (Fig. 24. e). This is reflected in the subsequent Sb_2Se_3 absorber as a layer consisting of large columnar and sintered grains aligned perpendicular to the substrate. Afterward, the SL deposition temperature was increased to 300 °C for further analysis. Almost a similar grain structure was observed for the main absorber film with a difference that the grains were not as uniform as the absorber with SL obtained at 280 °C. Herein, some grains were elongated more and had larger sizes (Fig. 24. g). Finally, 350 °C was used as the deposition temperature for the seed layer. Surprisingly, as can be seen in the top view image (Fig. 24. i), the Sb_2Se_3(SL) nanorods grains changed to platelike-shaped grains with sharp ends. This resulted in the fabrication of Sb_2Se_3 absorber with small grains with randomly oriented structure.

To gain more insight in the structure of the deposited Sb_2Se_3 absorber layers, films were analyzed by XRD. Figure 25. displays the XRD patterns of Sb_2Se_3/Sb_2Se_3(SL)/TiO_2/FTO/glass heterostructures with Sb_2Se_3(SL) deposited at different temperatures.

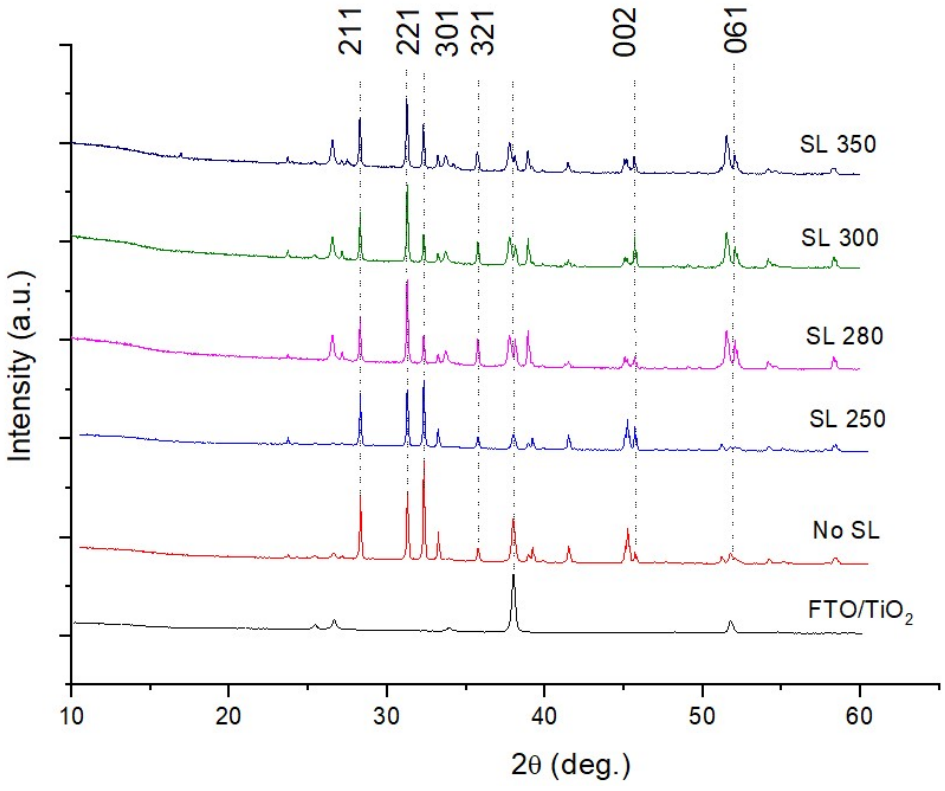

Fig. 25. XRD patterns of Sb_2Se_3/Sb_2Se_3(SL)/TiO_2/FTO/glass heterostructures with Sb_2Se_3(SL) deposited at different temperatures.

As can be seen, all the absorber layers are polycrystalline with dominant diffraction peaks corresponding to the orthorhombic Sb_2Se_3 crystal structure (PDF card no: JCPDS 01-089-0821) and matching well with those reported in the literature for Sb_2Se_3 films

deposited by CSS and VTD techniques. Among all the existing peaks, (221), (211) and (002) are the most representative as discussed in the literature. In addition, the undesired (120) peak which was often observed in several studies, was not observed in any of our fabricated films. This is a good indication since the presence of (120) peak would implies that the grains in the films lies parallel to the substrate. Thus, presence of intense (221) and (211) peaks, clearly indicate that the grains in the films are aligned perpendicular to the substrate. Such an alignment was previously shown that it is beneficial for efficient carrier transport [6] in the solar cell devices. Taking this to the consideration, the main attention was paid on the evolution of intensity for these three main peaks depending on the processing condition. For the absorber obtained with SL deposited at 250 ^{o}C, the XRD shows high intensity (301) peak, indicating that the absorber grains are relatively tilted. With increasing the deposition temperature of the SL to 280 ^{o}C, the intensity of the (301) peak drastically decreased, while the intensity of the (221) and (211) peaks became dominant. Further increasing the SL deposition temperature to 300 and 350 ^{o}C, the (221) direction and the (211) orientations remained the most dominant peaks. In addition to the main observed peaks, the presence of (002) peaks in all the films supports the columnar grain growth of the absorber layer.

3.1.2 Effect of Sb_2Se_3 seed layers by HVE

Section 3.1.2 describes the effect of Sb_2Se_3 seed layer deposited by HVE and its post-deposition treatment on the morphological and structural properties of CSS Sb_2Se_3 absorber layers in Sb_2Se_3(SL)/TiO_2/FTO/glass stack architecture. Figure 26 is presented to show top-view SEM images of the HVE Sb_2Se_3 (SL) and cross-sectional SEM images of Sb_2Se_3 thin film absorbers deposited onto HVE Sb_2Se_3(SL)/TiO_2/FTO/glass substrates.

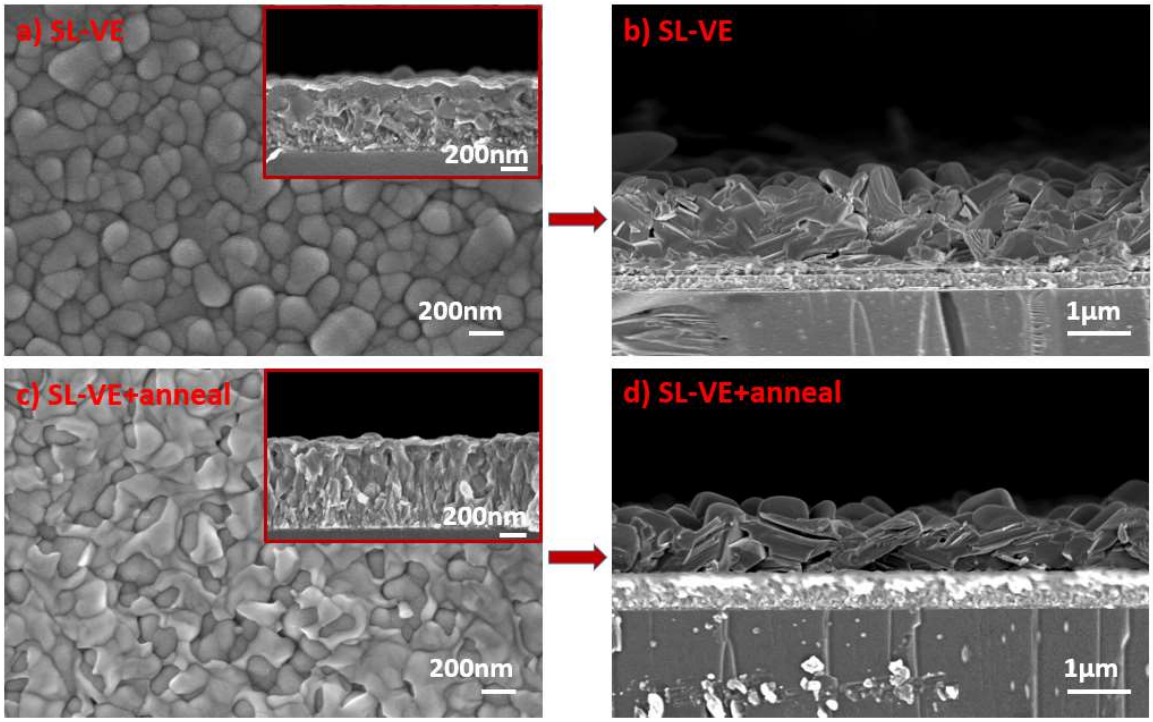

Fig. 26. SEM images of Sb_2Se_3 seed layers and Sb_2Se_3 thin film absorbers deposited onto TiO_2/FTO/glass and Sb_2Se_3(SL)/TiO_2/FTO/glass substrates by HVE and CSS, respectively. Left: top view (inset, cross-view) of (a) HVE as-deposited room temperature Sb_2Se_3 SL; (c) HVE Sb_2Se_3 SL annealed at 400 °C, 30 min in N_2 atmosphere. Right: (b and d) cross-sectional view of Sb_2Se_3 absorber films grown at 470 °C on corresponding Sb_2Se_3 SL (a and c).

Figure 26. a and 26. c present top view of the as-deposited Sb_2Se_3(SL) and Sb_2Se_3(SL) annealed at 400 °C for 30 min in N_2 atmosphere, respectively. As can be seen, the as deposited Sb_2Se_3 SL (Fig 26. a) covers uniformly the surface of TiO_2, following practically the relief of the TiO_2 rounded grains, which apparently look now larger due to the thickness of the seed. Such amorphous layer promoted in the next deposition step, an absorber film composed of large and relatively dense grains, but lying parallel on the TiO_2/FTO substrate (Fig 26. b). After post deposition annealing (Fig 26. c), the surface of SL turns to a network of weak contacted grains, which illustrates that a crystallization process took place in the result of this annealing step. According to the phase diagram of the Sb_2Se_3 [75], a significant mass loss occurs at 400 °C. This indicates that during the annealing at this temperature the films were crystalized via mass transport through the gas phase. However, since the SL is very thin (60-70 nm), the intensive recrystallization leads to formation of a network with weak contacted grains. Similar to as deposited SL, the crystalized one also promoted the formation of an absorber layer composed of grains lying parallel to the substrate (Fig 26. d).

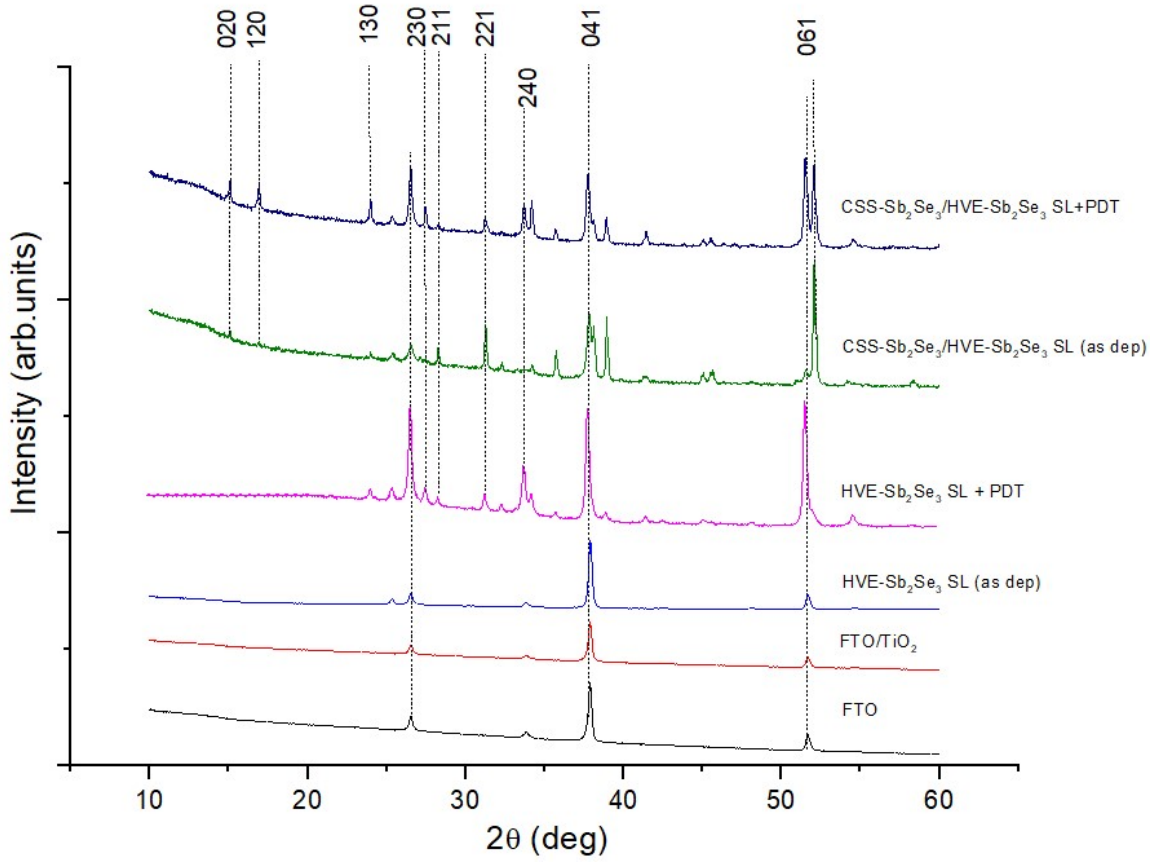

Fig. 27. XRD patterns of HVE Sb_2Se_3 SL/TiO_2/FTO, before and after PDT at 400 °C, 30 min in N_2, and Sb_2Se_3 absorber processed with these seed layers.

The analysis of the XRD patterns (Fig. 27.) supports the observation we had over the SEM images. The diffractogram of the HVE Sb_2Se_3 (SL) on top of TiO_2, does not contain any peaks related with Sb_2Se_3 material, indicating that the seed is amorphous (in agreement with SEM, Fig 26. a. After PDT at 400 °C, the peaks belonging to orthorhombic Sb_2Se_3 crystal structure appeared designating that a crystallization process occurred. As shown by SEM, after this annealing step a network of week contacted Sb_2Se_3 grains was clearly distinguished. After deposition of the absorber layer on top of as-deposited and annealed seeds, in addition to previously seen (221), (211) peaks, the diffractogram also shown a set of new peaks such as (020), (120), (130) and (230) with relatively high intensity. The presence of such intense peaks confirms the $(Sb_4Se_6)_n$ chains of seeds lying on the TiO_2/FTO substrate. It has been reported already that such orientation is not beneficial for the carrier transport in the Sb_2Se_3 thin film solar [28] [18]. Consequently, it is expected that the performance of the solar cells processed with those absorbers will be limited.

3.1.3 Effect of the Sb_2Se_3 absorber thickness

As shown above, the optimal seed layers which enabled fabrication of Sb_2Se_3 absorber layers with columnar sintered grains were obtained by CSS at 280 ^oC. Such growth protocol was optimized for the absorber films having thickness between 3-4 μm. A big challenge for the next step was to prove that by decreasing the thickness of the absorber it is possible to control and keep the columnar sintered grain feature of the films. To follow this approach, the thickness of the absorber was decreased from 4 to 1 μm and the changes in the absorber morphology was analyzed by SEM. Figure 28 shows SEM images of various thicknesses (4-1 μm) of CSS Sb_2Se_3 absorber layers deposited at 470 ^0C onto Sb_2Se_3(SL)/TiO_2/FTO/glass substrates, with CSS Sb_2Se_3 seeds grown at 280 ^0C (Fig. 24. c).

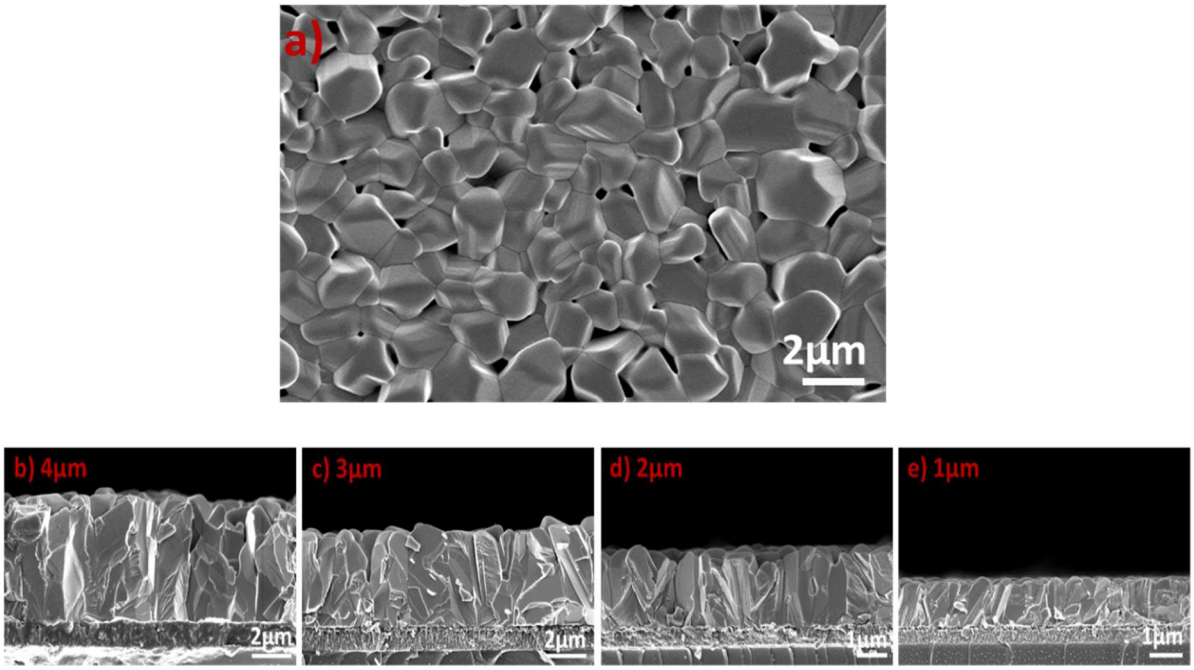

Fig. 28. SEM images of CSS Sb_2Se_3 absorber films deposited at 470 ^oC onto Sb_2Se_3(SL-280 ^oC)/TiO_2/FTO/glass substrates with different deposition time. a) top-view; b-e) cross-sectional view.

The captured top-view and cross-sectional SEM images of the deposited Sb_2Se_3 thin film absorber layers show the constant morphology of absorber as a function of its thickness. Sb_2Se_3 thin film absorber grains maintained their large size and uniform columnar shape when the thickness was reduced to 1 μm. This result is very promising as for 1D Sb_2Se_3 absorber material a thickness ≤1 μm is required for maximum light absorption and efficient carrier transport in the solar cell device.

3.1.4 The role and mechanism of seed layer in the growth of the Sb_2Se_3 absorber film

The differences in the grain structure, grain size, and orientation of the Sb_2Se_3 absorber layers deposited by CSS on top of TiO_2/FTO/glass substrates, with and without seed layers grown by CSS and HVE can be explained by differences in the nucleation density and coalescence rates at various processing conditions. According to the thin film growth theory, the initial seed layer plays a significant role in the final film orientation. Several reports in the literature revealed that [*hk0*] (*hkl* represents the Miller indices) orientations appeared in the Sb_2Se_3 absorber film when the TiO_2 was used as a buffer layer [75] [4]. The same effect was observed in this study where the Sb_2Se_3 absorber films processed without a seed layer exhibited dispersed structure with chaotically oriented grains (Fig. 24. a). At the same time, a number of reports showed a more controllable grain growth and [221] orientation (i.e., absence of [120] and [020]) of Sb_2Se_3 when deposited on CdS buffer layer. An explanation for the difference in the growth of the Sb_2Se_3 absorber on TiO_2 and CdS can be explained by the inert nature of TiO_2. The bond energy of Ti–O (662 kJ mol^{-1}) is much stronger than those of Cd–S (196 kJ mol^{-1}), thus, the Sb and Se are difficult to bond with TiO_2 substrate during the film deposition, resulting in most of the $(Sb_4Se_6)_n$ chains lying on the substrate [75]. Following this logic, two very recent reports by Hutter *et al*. [6] and by Li *et al*. [75] showed the application of a seed layer as an efficient technological approach to control the growth of Sb_2Se_3 thin film absorber. In [6] , it was shown that a CSS Sb_2Se_3 seed layer grown with a source temperature of 350 °C is optimal for the growth of compact and dense CSS Sb_2Se_3 absorber film, leading to a 6.6% solar cell efficiency. However, a very important technological parameter, the CSS substrate temperature, was not disclosed in that paper. In [75], a systematic approach of seed layer screening by rapid thermal evaporation (RTE) at 420 °C for different time (between 0 and 1000 s) was used to develop compact [221] oriented Sb_2Se_3 absorber films achieving the same 6.6% device efficiency.

In contrast with the reported results, in the current study, the optimal seed layer, which promoted in the subsequent deposition step an [221] oriented Sb_2Se_3 absorber film with columnar sintered grains, was obtained by CSS at 280 °C. The explanation for the beneficial effect of this seed layer is related to its nanorod grain structure at this temperature. During CSS of Sb_2Se_3 seed at 280 °C the adatom surface diffusion on the surface of TiO_2 is quite significant, resulting in local epitaxial growth on individual grains. The grain coarsening occurs during the coalescence of small islands with large surface-to-volume ratios, whereas GBs become immobile in continuous layers [52]. A pronounced columnar structure develops, in which the columns are actually elongated

nanorods. The nanorod structure acts as a seed layer for the subsequent grain growth at the higher temperature of 460 °C. At this high temperature, the adatoms are very mobile on the surface, and a complete coalescence will occur for relatively large islands because the rate of material transfer between islands is high. GB migration takes place not only during coalescence but throughout the film-thickening process. Thus, large Sb_2Se_3 columnar grains with low surface energies grow in both perpendicular and lateral directions, leading to the formation of a dense, continuous, and [221] oriented Sb_2Se_3 absorber layers.

3.2 Solar cell performance

Section 3.2.1 and 3.2.2. report on the impact of Sb_2Se_3 absorber processed with different seed layers and the effect of absorber thickness on the performance of Au/Sb_2Se_3/Sb_2Se_3(SL)/TiO_2/FTO/glass solar cells. Herein, the main photovoltaic parameters of the fabricated thin film solar cells were measured under AM1.5 conditions.

3.2.1 Effect of Sb_2Se_3 seed layer deposition condition on solar cells performance

Table 1 illustrates that using CSS for deposition of Sb_2Se_3 seed layers results in the fabrication of considerably much more efficient Au/Sb_2Se_3/Sb_2Se_3(SL)/TiO_2/FTO/glass solar cells compared to the devices where their seed layers are deposited by HVE.

Table 1. Photovoltaic parameters of glass/FTO/TiO_2/ Sb_2Se_3(SL)/Sb_2Se_3/Au solar cells processed with Sb_2Se_3 seed layers (SL) by CSS and HVE.

	Seed Layer (SL)	V_{OC} [mV]	J_{SC} [mA/cm^2]	FF [%]	PCE [%]	R_S [Ωcm^2]	R_{SH} [Ωcm^2]
CSS-SL	No SL	240±10	19.5±0.5	35±3	1.6±0.3	18±5	290±38
	SL-250 °C	340±10	22.6±0.5	42±3	3.2±0.3	12±5	480±90
	SL-280 °C	390±10	24.5±0.3	48±2	4.6±0.3	8.8±4	1000±270
	SL-300 °C	380±10	23.8±0.3	47±2	4.2±0.3	9.5±7	820±230
	SL-350 °C	270±10	22.5±0.5	38±3	2.31±0.3	22±6	370±120
HVE-SL	SL-as deposited	260±10	10.7±0.5	35±3	1.0±0.3	32±15	350±60
	SL-annealed at 400 °C, at N_2 for 20 min	100±10	10.1±0.5	32±3	0.32±0.3	39±8	245±100

The low PCE of the solar cells was largely determined by low $J_{SC,}$ and this can be attributed to the Sb_2Se_3 absorber grains being aligned in parallel to the surface. HVE SL was not successful in providing the required condition for the growth of Sb_2Se_3 absorber, and therefore, samples made by this approach were not studied further.

As can be seen in the table, the changes made into the main PV parameters of $Au/Sb_2Se_3/Sb_2Se_3$(SL)$/TiO_2/FTO$/glass solar cells fabricated with Sb_2Se_3 seed layers through CSS can be divided into two stages, based on Sb_2Se_3 seed layer deposition temperature. In the first stage, the deposition of Sb_2Se_3 seed layer and increasing its deposition temperature up to 280 °C, significantly enhanced the performance of the device and resulted in higher values of V_{OC}, J_{SC}, FF, and PCE. Herein, the V_{OC}, J_{SC}, FF, and PCE of the No SL device increased from 240 mV, 19.5 mA/cm^2, 35.3%, and 1.6% to 340 mV, 22.6 mA/cm^2 to 42.3%, and 3.2% through deposition of seed layer at 250 °C, respectively. Further increase of the deposition temperature to 280 °C, resulted in recording the best-performing device. The SL-280 device generated the highest V_{OC}, J_{SC}, FF with the values of 390 mV, 24.5 mA/cm^{2,} and 48.2%, respectively. Thus, the highest PCE of 4.6% was achieved. This trend in the evolution of PV parameters was also supported by the changes made in R_S and R_{SH}. As can be seen, deposition of Sb_2Se_3(SL) and further increasing its deposition temperature up to 280 °C, reduced R_S, increased FF and R_{SH} of the device. This is a desirable trend as for an ideal solar cell as R_S should always tend to zero and R_{SH} should tend to infinite. The current-voltage (J-V) characteristics of the $Au/Sb_2Se_3/Sb_2Se_3$(SL-280)$/TiO_2/FTO$/glass solar cell is presented in Figure 29.

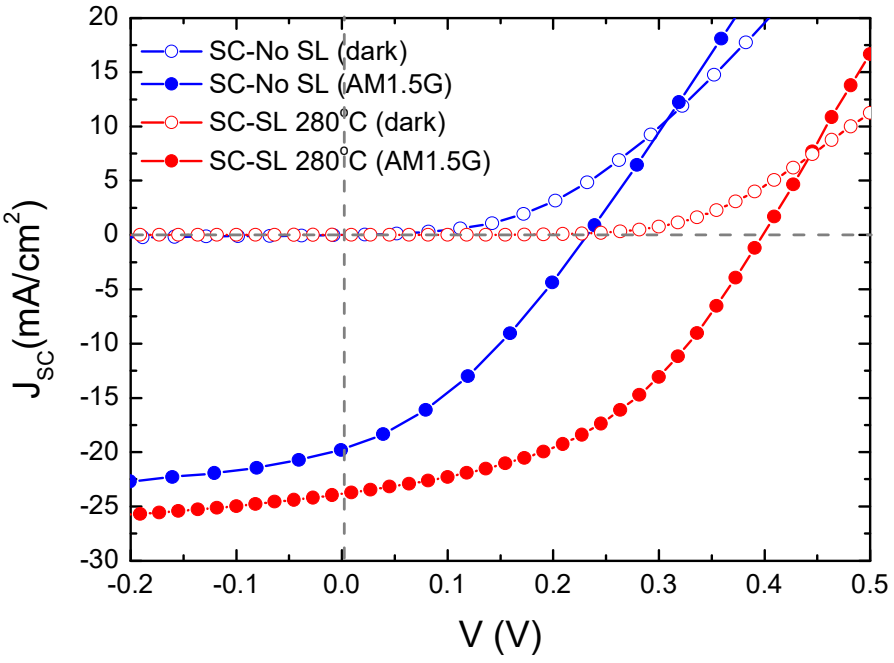

Fig. 29. Current-voltage characteristics (*J-V*) measured in dark and at AM1.5G of Sb_2Se_3 solar cells without seed layer (blue curves), and with optimal seed layer obtained by CSS at 280 °C (red curves).

In the second stage, when the Sb_2Se_3(SL) deposition temperature increased to 300 °C, PCE decreased slowly to 4.2% (at 300 °C) and with further increase of the temperature to 350 °C the PCE drastically dropped to 2.31%. The low PCE of solar cells obtained at 350 °C was largely determined by a sudden drop in the V_{OC}, reaching its lowest value of 270 mV among all devices with CSS Sb_2Se_3 seed layer.

When explaining the impact of Sb_2Se_3(SL) CSS deposition condition on the Au/Sb_2Se_3/Sb_2Se_3(SL)/TiO_2/FTO/glass solar cell device performance, changes in the structural properties of Sb_2Se_3 should be considered. It is known that the grain size and orientation have a major impact on device performance, and devices with smaller Sb_2Se_3 absorber grains generate lower PCE. This happens since small grains in the films imply the presence of high-density GBs. Thus, results in higher recombination losses and a lower lifetime of the photogenerated minority carriers. The effect of higher recombination losses in the main PV parameters can be observed in the higher dark current (I_o) and lower V_{OC}. Considering this, the low measured values of V_{OC} and PCE for No-SL and SL-350 solar cells can be explained by random absorber structure and small grain sizes.

External Quantum Efficiency (EQE) of the Au/Sb_2Se_3/Sb_2Se_3(SL-280)/TiO_2/FTO/glass and Au/Sb_2Se_3/Sb_2Se_3(No-SL)/TiO_2/FTO/glass solar cells are given in Fig. 30.

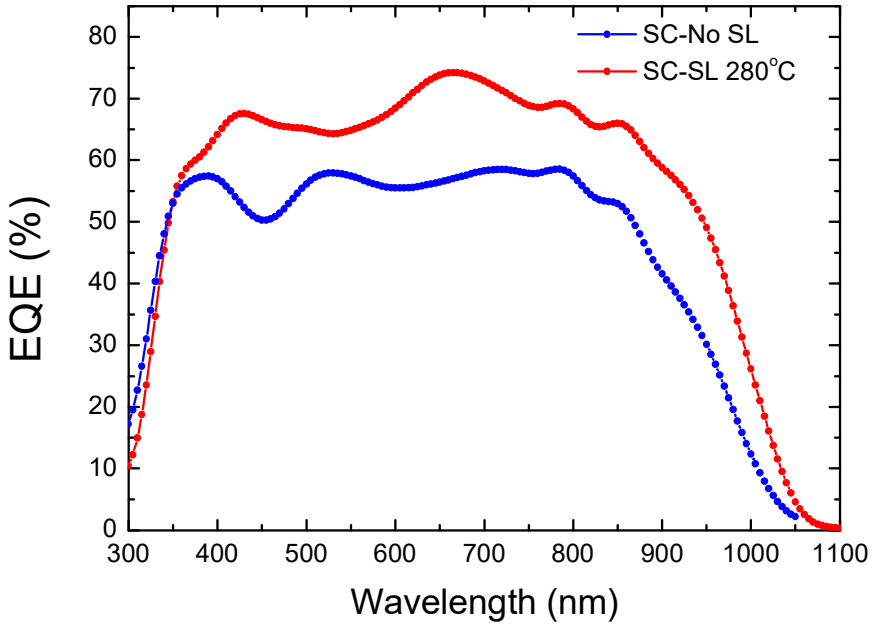

Fig. 30. External quantum efficiency (EQE) of Sb_2Se_3 solar cells without seed layer (blue curve), and with optimal seed layer obtained by CSS at 280 °C (blue curve).

The EQE supports the above conclusions. The device with the highest PCE, obtained with SL-280 °C shows the highest spectral response through the entire 350-1000 nm

wavelength range, indicating to the efficient carrier transport and better collection efficiency. For the device without seed layer the EQE response decreased in the entire wavelength interval. This effect is explained by the short carrier diffusion length, most probably due to recombination at the GBs which were present in a high concentration in the Sb_2Se_3 absorber layer deposited without seed layer.

3.2.2 Effect of Sb_2Se_3 absorber thickness on the best performing solar cell

This section describes the effects of Sb_2Se_3 absorber thickness on performance of the Au/Sb_2Se_3/Sb_2Se_3(SL)/TiO_2/FTO/glass solar cell fabricated with Sb_2Se_3 SL-280. Herein, the best performing device (the SL-280 structure) was chosen for analysis.

Table 2. Photovoltaic parameters of glass/FTO/TiO_2/Sb_2Se_3(SL)/Sb_2Se_3/Au processed with CSS Sb_2Se_3 SL-280°C and varying the thickness of the Sb_2Se_3 absorber layer from 4μm to 1μm.

	Sb_2Se_3 absorber thickness	V_{OC} [mV]	J_{SC} [mA/cm²]	FF [%]	PCE [%]	R_S [Ωcm²]	R_{SH} [Ωcm²]
CSS SL-280°C	4 μm	380±10	22.5±0.3	42±2	3.6±0.3	14±8	670±330
	3 μm	390±10	23.4±0.3	48±2	4.4±0.3	9.2±4	1000±270
	2 μm	410±10	24.5±0.3	49±2	4.9±0.3	8.7±6	1400±135
	1 μm	360±10	25.8±0.3	52±2	4.8±0.3	7.5±3	1500±160

Measured J–V parameters, including PCE, are shown in Table 2. As can be seen, reducing the absorber thickness from 4 to 1 μm resulted to higher J_{SC}. Thus, the highest J_{SC} was recorded for 1 μm thickness with a value of 25.8 mA/cm^2. The increasing trend of J_{SC} was expected as recombination losses decrease when the absorber layer thickness reduces. In the Sb_2Se_3 absorbers with lower thickness, charge carriers need to move shorter distances to be extracted and, therefore, are more likely to not end up with recombination. On the other hand, the same trend was observed for the V_{OC} which gradually increased from 380 to 410 mV when the absorber thickness decreased from 4 to 2 μm. An unexpected result is that for 1 μm absorber thickness the V_{OC} dropped drastically to 360 mV. This effect is not clear yet but it might indicate that there is a trade-off between the minimum desired absorber thickness and maximum achievable PV parameters and PCE. At the same time, theoretically it was shown that higher than 10% PCE devices can be obtained with Sb_2Se_3 absorber film thickness ≤1 μm [33]. This indicates that further systematic studies are required to develop and optimize efficient Sb_2Se_3 devices with absorber thickness ≤1 μm.

CONCLUSION

This work is focused on optimization of Sb_2Se_3 thin film absorber growth protocol via controlling Sb_2Se_3 seed layer processing conditions. Herein, the Sb_2Se_3(SL) was deposited at various conditions by CSS and HVE. The effect of Sb_2Se_3(SL) deposition conditions on growth of the close-spaced sublimated Sb_2Se_3 absorber layer was studied through SEM and XRD analysis. The correlation between Sb_2Se_3 thin film absorber growth, thickness and the Au/Sb_2Se_3/Sb_2Se_3(SL)/TiO_2/FTO/glass solar cells performance was studied.

The study resulted in gaining a broader knowledge of thin film solar cell working principle, deposition methods such as close-spaced sublimation and Ultrasonic spray pyrolysis, as well as material and device characterization techniques such as SEM, XRD, EQE and J-V curve measurements. The following results and conclusions are concluded:

1. Sb_2Se_3 seed layer considerably affects the structural and morphological properties of the subsequently deposited absorber layer. Sb_2Se_3 seed layers, depending on deposition temperature and the deployed deposition method, provides nucleation sites for Sb_2Se_3 absorber grains to grow. Deposition of Sb_2Se_3(SL) by CSS was significantly more effective than HVE to reach to higher PCE. The subsequently grown Sb_2Se_3 absorber layer on HVE SL had small grains and was randomly oriented. Deposition of Sb_2Se_3(SL) by CSS at 250 ^oC, relatively enlarged, and aligned Sb_2Se_3 absorber grains perpendicular to the surface. Further increasing the seed layer deposition temperature to 280 and 300 ^oC, resulted in the fabrication of larger grains and more uniformly aligned absorber structure. Sb_2Se_3 seed layer deposition at temperatures more than these values were destructive for absorber growth.

2. Photovoltaic performance of Au/Sb_2Se_3/Sb_2Se_3(SL)/TiO_2/FTO/glass solar cells was correlated to the structural and morphological properties of the Sb_2Se_3 absorber layer. Since the Sb_2Se_3 absorber layer itself was affected by the seed layer, consequently, the solar cell performance was correlated to the deposition condition of the Sb_2Se_3 seed layer. The best solar cell performance was attributed to the best Sb_2Se_3 absorber layer quality. The best absorber quality was achieved for Sb_2Se_3/CSS Sb_2Se_3(SL)/TiO_2/FTO/glass where the seed layer was deposited at 280 ^oC (SL-280). The deposition of the seed layer at 280 ^oC improved the grain growth of the Sb_2Se_3 absorber layer and resulted in uniformly oriented and large columnar grains. Grains were aligned upwards and perpendicular to the surface. The solar cell showed consistent EQE of more than 60% over a broad region of 380 to 900 nm and recorded the PCE of 4.6%.

3. It was demonstrated that decreasing the absorber thickness from 4 to 1 micron, the columnar grain growth protocol is maintained and controlled. The effect of absorber thickness on CSS Sb_2Se_3(SL-280)/TiO_2/FTO/glass solar cell performance was analyzed. It was shown that decreasing the absorber thickness resulted in higher J_{SC} and PCE. This was contributed to Higher R_{SH} lower R_S and recombination losses when the thickness is decreased. 2 μm absorber thickness was found to be the optimal thickness for the maximum PCE.

SUMMARY

Photovoltaics (PV) is an important key renewable technology that can help to meet the world's growing energy demand without endangering our environment. Meanwhile, more efficient and cost-effective technologies must be developed in order to make PV technologies competitive in the energy market.

Antimony selenide is a promising photovoltaic absorber material due to its suitable bandgap, high absorption coefficient, long carrier lifetime, and decent carrier mobility. Sb_2Se_3 is made of earth-abundant, non-toxic compounds, possess high vapor pressure, and low melting temperature. It can be fabricated by deposition techniques that have already been used to fabricate CdTe solar cells.

In this work, I focused on optimization of Sb_2Se_3 thin film absorber growth protocol and its application in solar cells. The effect of Sb_2Se_3 seed layer deposition condition on the structural and morphological properties of the Sb_2Se_3 seed layer deposited onto TiO_2/FTO/glass substrate was studied, and then, it was investigated how the growth history of the seed layers influences the grain growth of subsequent CSS Sb_2Se_3 thin film absorber layers.

The best Sb_2Se_3 seed layer deposition condition was determined by the deposition of various seed layers being deposited by CSS or HVE at 250 to 350 ^oC. It was revealed that seed layer deposition at 280 ^oC and through CSS technique produced large absorber crystal grains and the most uniform structure. This resulted in Au/Sb_2Se_3/Sb_2Se_3(SL-280)/TiO_2/FTO/glass solar cells attaining the highest PCE of 4.2%.

The effect of Sb_2Se_3 absorber thickness on the best performing Au/Sb_2Se_3/Sb_2Se_3(SL-280)/TiO_2/FTO/glass solar cells was further studied. Sb_2Se_3 absorber showed constant morphology as a function of its thickness, and absorber grains maintained their large size and uniform columnar shape when the thickness was changed. It transpired that the optimal absorber thickness of 2 μm (in 4 to 1 μm range) resulted in the best device performance. We attributed this to lower recombination losses and lower resistance. Herein, our Au/Sb_2Se_3/Sb_2Se_3(SL-280)/TiO_2/FTO/glass solar cells solar cell with Sb_2Se_3 absorber thickness of 2 μm produced the highest PCE of 4.9%

4 REFRENCES

[1] X. Liu, J. Chen, M. Luo, M. Leng, Z. Xia, Y. Zhou, S. Qin, D.-J. Xue, L. Lv, H. Huang, D. Niu and J. Tang, "Thermal Evaporation and Characterization of Sb2Se3 Thin Film for Substrate Sb2Se3/CdS Solar Cells," *ACS Applied Materials & Interfaces,* 2014.

[2] W. Wang, L. Dong, J. Wang, X. Shi and S. Han, "Characterization and photocatalytic activity of mesoporous TiO2 prepared from an ethanol–diethyl ether binary solvent system," Chemical Physics Letters, 2014.

[3] P. Sinsermsuksakul, K. Hartman, S. B. Kim, J. Heo, L. Sun, H. H. Park, R. Chakaraborty, T. Buonassisi and R. G. Gordon, "Enhancing the efficiency of SnS solar cells via band-offset engineering with a zinc oxysulfide buffer layer," Applied Physics Letters, 2013.

[4] Z. Li, X. Liang, G. Li, H. Liu, H. Zhang, J. Guo, J. Chen, K. Shen, X. San, W. Yu, R. Schropp and Y. Mai, "9.2% Efficient Core shell Structured Antimony Selenide Nanorod Array Solar Cells," Nature Commiunications, 2019.

[5] W. Xixing, C. Chao, L. Shuaicheng, L. Kanghua, K. Rokas, Z. Yang, C. Wenhao, G. Liang, W. Chong, Z. Jun, N. Guangda and T. Jiang, "Vapor transport deposition of antimony selenide thin film solar cells with 7.6% efficiency," Nature Communications, 2018.

[6] O. S. Hutter, L. J. Phillips and K. Durose and J. D. Major, "6.6% efficient antimony selenide solar cells using grain structure control and an organic contact layer," Solar Energy Materials and Solar Cells, pp. 177-181, 2018.

[7] H. Shiel, O. S. Hutter, L. J. Philips, M. Al Turkestani, V. R. Dhanak, T. D. Vea, K. Durose and J. D. Major, "Chemical etching of Sb2Se3 solar cells: surface chemistry and back contact behaviour," JPhys Energy, 2019.

[8] R. Gomez and J. L. Segura, "Plastic Solar Cells: A Multidisciplinary Field To Construct Chemical Concepts from Current Research," Journal of chemical education, 2007.

[9] U. Mishra and J. Singh, Semiconductor Device Physics and Design, Dordrecht: Springer, 2007.

[10] K. Ranabhat, L. Patrikeev, A. A. Revina, K. Andrianov, V. Lapshinsky and E. Sofronova, "AN INTRODUCTION TO SOLAR CELL TECHNOLOGY," Journal of Applied Engineering Science, 2016, pp. 481-485.

[11] M. T. Kibria, A. Ahammed, S. M. Sony, F. Hossain and S. Ul slam, "A Review: Comparative studies on different generation solar cells technology," Proceedings of 5th International Conference on Environmental Aspects of Bangladesh, 2014.

[12] T. D. Lee, A. U. Ebong, "A review of thin film solar cell technologies and challenges," Renewable and Sustainable Energy Reviews, 70, 1286–1297, 2017.

[13] M. Uurike, "Influence of pH on the properties of chemically deposited CdS thin films and solar cells," Tallinn: TUT Press, 2017.

[14] G. Stechmann, S. Zaefferer, P. Konijnenberg, D. Raabe, C. Gretene, L. Kranz, J. Perrenoud, S. Buecheler and A. N. Tiwari, "3-Dimensional microstructural characterization of CdTe absorber layers from CdTe/CdS thin film solar cells," Solar Energy Materials & Solar Cells, 2016.

[15] "2019 United Nations Framework Convention on Climate Change," The Paris Agreement, October 2018.

[16] J. S. Eensalu, A. Katerski, E. Kärber, I. O. Acik, and A. Mere and M. Krunks, "Uniform Sb2S3 optical coatings by chemical spray method," eilstein Journal of Nanotechnology, pp. 198-210, 2019.

[17] H. A. Atwater and A. Polman, ""Plasmonics for improved photovoltaic devices," Nature Materials, pp. 205-213, 2010.

[18] C. Chen, D. C. Bobela, Y. Yang, S. Lu, u, K. Zeng, C. Ge, B. Yang, L. Gao and Y. Zhao, M. C. Beard and J. Tang, ""Characterization of basic physical properties of Sb2Se3 and its relevance for photovoltaics," Frontiers of Optoelectronics, pp. 18-30, 2017.

[19] S. Paul, R. Lopez, M.D. Mia, C.H. Swartz and J.V. Li, "A Simulation Study on Radiative Recombination Analysis in CIGS Solar Cell," in 2017 IEEE 44th Photovoltaic Specialist Conference (PVSC), 2018.

[20] A. Goetzberger, J. Knobloch and B. Voss, Crystalline Silicon Solar Cells, 1998.

[21] F. Staub, U. Rau and T. Kirchartz, "Statistics of the Auger Recombination of Electrons and Holes via Defect Levels in the Band Gap—Application to Lead-Halide Perovskites," ACS OMEGA, 2018.

[22] P. Würfel, Physics of Solar Cells: From Principles to New Concepts, 2005.

[23] J. D. Puksec, "Recombination Processes and Holes and Electrons Lifetimes," AUTOMATIKA 43(2002), 2002.

[24] T. Goudon, V. Miljanovi and C. Schmeiser, "On the Shockley-Read-Hall Model:Generation-Recombination in Semiconductors," SIAM Journal on Applied Mathematics, 2006.

[25] J. Nelson, "The Physics of Solar Cells," Imperial College Press, 2003.

[26] W. Liang, L. D. Bing, L. Kanghua, C. Chao, D. Hui-Xiaong, G. Liang, Z. Yang, J. Fan, L. Luying, H. Feng, H. Yisu, S. Haisheng, N. Guangda and T. Jiang, "Stable 6%-effcient Sb2Se3 solar cells with a ZnO buffer layer," Nature Energy, 2017.

[27] L. Wang, M. Luo, S. Qin, X. Liu, J. Chen, B. Yang, M. Leng, D.-J. Xue, Y. Zhou, L. Gao, H. Song and J. Tang, "Ambient CdCl2 Treatment on CdS Buffer Layer for Improved Performance of Sb2Se3 Thin Film Photovoltaics," Applied Physics Letters, 2015.

[28] Z. Ying, W. Liang, C. Shiyou, Q. Sikai, L. Xinsheng, C. Jie, X. Ding-Jang, L. Miao, C. Yuanzhi, C. Yibing, H. S. Edward and T. Jiang, "Thin-film Sb2Se3 photovoltaics with oriented one-dimensional ribbons and benign grain boundaries," Nature Photonics, 2015.

[29] L. J. Phillips, C. N. Savory,, P. J. Yates,, O. S. Hutter, H. Shiel, S. Mariotti, L. Bowen, M. Birkett and K. Durose, D. O. Scanlon and J. D. Major, "Current Enhancement via a TiO2 Window Layer for CSS Sb2Se3 Solar Cells: Performance Limits and High Voc," IEEE Journal of Photovoltaics, 2019.

[30] S. Messina, M. T. S. Nair and P. K. Nair, "Antimony Selenide Absorber Thin Films in All-Chemically Deposited Solar Cells," Journal of The Electrochemical Society, 2009.

[31] Y. C. Choi, T. N. Mandal, W. S. Yang, Y. H. Lee, S. H. Im, J. H. Noh and S. Seok, "Sb2Se3-sensitized inorganic–organic heterojunction solar cells fabricated using a s single-source precursor," Angewandte Chemie, 2015.

[32] C. Chen, L. Wang, L. Gao, D. Nam, H. Cheong, K. Liu, H. Song, J. Tang, D. Li, K. Li, Y. Zhao and G. Ge, "6.5% certified efficiency Sb2Se3 solar cells using PbS colloidal quantum dot films as hole-transporting layer," ACS Energy Lett. 2, 2017.

[33] T. D. C. Hobson, L. J. Philips, O. S. Hutter, H. Shiel, J. E. N. Swallow, C. N. Savory, P. K. Nayak, S. Mariotti, B. Das, L. Bowen, L. A. H. Jones, T. J. Featherstone, M. J. Smiles, M. A. Farnworth, G. Zoppi, P. K. Thakur, T. L. Lee, H. J. Snaith, C. Leighton, D. O. Scanlon, V. R. Dhanak, K. Durose, T. D. Veal and J. D. Major, "Isotype Heterojunction Solar Cells Using n-Type Sb2Se3 Thin Films," Chemistry of Materials, 2020.

[34] G. Li, Z. Li, X. Chen, S. Qiao, S. Wang, Y. Xu and Y. Mai, "Self-powered, high-speed Sb2Se3/Si heterojunction photodetector with close spaced sublimation processed Sb2Se3 layer," Journal of Alloys and Compounds, 2018.

[35] Z Chen, I Dündar, I Oja Acik and A Mere, "TiO2 thin films by ultrasonic spray pyrolysis," in IOP Conf. Series: Materials Science and Engineering 503, 2019.

[36] T Ivanova, A Harizanova, T Koutzarova, B Vertruyen, "Characterization of nanostructured TiO2: Ag films: structural and optical properties," Journal of Physics Conference Series, vol. 764, pp. 12-19, 2016.

[37] S. Mahalingam and M. J. Edirisinghe, "Characteristics of electrohydrodynamically prepared titanium dioxide films," Applied physics a-materials science & processing, pp. 987-993, 2007.

[38] Mahalingam S and Edirisinghe M J, "Characteristics of electrohydrodynamicallyprepared titanium dioxide films," Applied Physics A: Materials Science & Processing, 2007.

[39] S. Paul and A. Choudhury, "Investigation of the optical property and photocatalytic activity of mixed phase nanocrystalline titania," Applied nanoscience, pp. 839-847, 2014.

[40] D. Perednis and L. J. Gauckler, "Thin Film Deposition Using Spray Pyrolysis," Journal of Electroceramics, pp. 103-111, 2005.

[41] O. O. Abegunde, E. T. Akinlabi, O. P. Oladijo, S. Akinlabi and A. U. Ude, "Overview of thin film deposition techniques," Material Science, 2019.

[42] G. C. Righini and A. Chiappini, "Glass optical waveguides: a review of fabrication techniques," Optical Engineering, 2014.

[43] A. Conde-Gallardoa, M. Guerrero, N. Castillo, A. B. Soto, R. Fragoso and J. G. Caban, "Thin Solid Films," TiO2 anatase thin films deposited by spray pyrolysis of an aerosol of titanium diisopropoxide, pp. 78-73, 2015.

[44] K. A. Aadim, K. Haneen and Q. M. Hadi, "Effect of Annealing Temperature on the Optical Properties of TiO2 Thin Films Prepared by Pulse Laser Deposition," International Letters of Chemistry, Physics and Astronomy, 2015.

[45] I. Vaiciulis, M. Girtan, A. I. Stanculescu, L. Leontie, F. Habelhames and S. Antohe, "On titanium oxide spray deposited thin films for solar cells applications," The publishing house of the romainian academy, pp. 335-342, 2012.

[46] V. Zharvan, R. Daniyati, N. Ichzan and G. Yudoyono, "Study on fabrication of TiO2 thin films by spin-coating and their optical properties," AIP Conference Proceedings, 2016.

[47] I. Senain, N. Nayan and H. Saim, "Structural and Electrical Properties of TiO2 Thin Film Derived from Sol-gel Method using Titanium (IV) Butoxide," Intergrated engineering, 2010.

[48] I. Karabay, S. Aydın Yüksel, F. Ongül, S. Öztürk and M. Asli, "Structural and Optical Characterization of TiO2 Thin Films Prepared by Sol–Gel Process," Applied Physics and Materials Science, 2012.

[49] N. Amin and K.S. Rahman, "Close-Spaced Sublimation (CSS): A Low-Cost, High-Yield Deposition System for Cadmium Telluride (CdTe) Thin Film Solar Cells," in Modern Technologies for Creating the Thin-film Systems and Coatings, Intech, 2017.

[50] L.J. Philips, P. Yates, O.S. Hutter, T. Baines, L. Bowen, K. Durose and J.D. Major, "Close-Spaced Sublimation for Sb2Se3 Solar Cells," in IEEE PVSC 44, 2017.

[51] D. Rose, F. Hasoon, R. G. Dhere, D. S. Albin, R. M. Ribelin, X. Li and Y. Mahathongdy, "Fabrication procedures and process sensitivities for CdS/CdTe solar cells," Progress in Photovoltaics Research and Applications, 1999.

[52] N. Spalatu, Development of CdTe Absorber Layer for Thin-Film Solar Cells, Tallinn: TTU Press, 2017.

[53] M. Krunks, O. Kijatkina, H. Rebane, I. Oja, V. Mikli and A. Mere, "Composition of CuInS2 thin films prepared by spray pyrolysis," Thin Solid Films, Vols. 403-404, pp. 71-75, 2002.

[54] O. Malik, F. J. De La Hidalga-Wade and R. R. Amador, "Spray Pyrolysis Processing for Optoelectronic Applications," InTech, 2017.

[55] C. Falcony, M. A. Aguilar-Frutis and M. G. Hipolito, "Spray Pyrolysis Technique; High-K Dielectric Films and Luminescent Materials: A Review," Micromachines, 2018.

[56] V. K. Singh, "Thin Film Deposition By Spray Pyrolysis Techniques," Journal of Emerging Technologies and Innovative Research, vol. 4, no. 11, 2017.

[57] R. Suresh, V. Ponnuswamy and R. Mariappan, "Effect of solvent and substrate temperature on morphology of cerium oxide thin films by simple nebuliser spray pyrolysis technique," Materials Technology, pp. 12-22, 2014.

[58] A. A. Bunaciu, E. G. Udristioiu and H. Y. Abdoul-Enein, "X-Ray Diffraction: Instrumentation and Applications," Critical Reviews in Analytical Chemistry 45 (4): 289–99, 2015.

[59] J.P. Patel and P.H. Parsania, "Characterization, Testing, and Reinforcing Materials of Biodegradable Composites," in Biodegradable and Biocompatible Polymer Composites, Woodhead Publishing Series in Composites Science and Engineering, 2018, pp. 55-79.

[60] B. D. Fahlman, Materials Chemistry, Springer Netherlands, 2011.

[61] A. R. West, Solid State Chemistry and its Application, John Wiley & Sons Ltd, 1984.

[62] V. K. Sharma and K. Mahendra, "Scanning Electron Microscopy (SEM) of Multilayer CDS Thin Films," International Journal for Research in Applied Science & Engineering Technology(IJRASET), 2014.

[63] [Online]. Available: https://blog.phenom-world.com/what-is-sem.

[64] P. Wandrol, J. Matejkova and A. Rek, "High Resolution Imaging by Means of Backscattered Electrons in the Scanning Electron Microscope," Materials Science Forum, 2007.

[65] K. Kersten, "The Phenom Process Automation: mixing backscattered and secondary electron images using a Python script," Thermo Fischer Scientific, 2018.

[66] P. W. Hawkes and J. C. H. Spence, Science of Microscopy, New York: Springer, 2007.

[67] GVS Apoorva, T. G. Manohar and Uma BR, "Performance Characteristics of Solar Cells in Spaceunder Shadow Effect," International Journal of Engineering Research and Application, 2017.

[68] E. Durán, J. M. Andújar, J. M. Enrique and J. M. Pérez-Oria, "Determination of PV Generator I-V/P-V Characteristic Curves Using a DC-DC Converter Controlled by a Virtual Instrument," International Journal of Photoenergy, 2011.

[69] L. Cojocaru, S. Uchida, K. Tamak, P. V. V. Jayaweera, S. Kaneko, J. Nakazaki, T. Kubo, T. Kubo and H. Segawa, "Determination of unique power conversion efficiency of solar cell showing hysteresis in the I-V curve under various light intensities," Scientific Reports, 2017.

[70] A. Wisnu, "External quantum efficiency measurement of solar cell," in 15th International Conference on Quality in Research (QiR) : International Symposium on Electrical and Computer Engineering, 2017.

[71] W.J.Yang, Z.Q.Ma, X.Tang, C.B.Feng, W.G.Zhao and P.P.Shi, "Internal quantum efficiency for solar cells," Solar Energy, pp. 106-110, 2008.

[72] "PVEducation.org," [Online]. Available: https://www.pveducation.org/pvcdrom/solar-cell-operation/quantum-efficiency.

[73] B. Hussain and A. Ebong, "Specifications of ZnO growth for heterostructure solar cell and PC1D based simulations," Data in Brief, 2015.

[74] I. Dundar, M. Krichevskaya, A. Katerski and I. O. Acik, "TiO2 thin films by ultrasonic spray pyrolysis as photocatalytic material for air purification," Royal Society Open Science, 2019.

[75] K. Li, C. Chen, S. Lu, C. Wang, S. Wang, Y. Lu and J. Tang, "Orientation Engineering in Low-Dimensional Crystal-Structural Materials via Seed Screening," Advanced Materials, 2019.